Biomaterials Advances 166 (2025) 214036

Contents lists available at ScienceDirect

Biomaterials Advances

journal homepage: www.journals.elsevier.com/materials-science-and-engineering-c

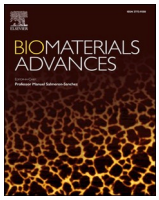

Core-shell electrospun polycaprolactone nanofibers, loaded with rifampicin and coated with silver nanoparticles, for tissue engineering applications

Luigi Musciacchio [a,1], Mario Mardirossian [a,2], Giovanna Marussi [b], Matteo Crosera [b], Gianluca Turco [a], Davide Porrelli [a,*,3]

[a] Department of Medicine, Surgery and Health Sciences, University of Trieste, Piazza dell'Ospitale 1, 34125 Trieste, Italy
[b] Department of Chemical and Pharmaceutical Sciences, University of Trieste, Via Licio Giorgieri 1, 34127 Trieste, Italy

ARTICLE INFO

Keywords:
Antibacterial
Antimicrobial peptides
Core-shell nanofibers
Electrospinning
Biomaterial
Tissue engineering

ABSTRACT

In the field of tissue engineering, the use of core-shell fibers represents an advantageous approach to protect and finely tune the release of bioactive compounds with the aim to regulate their efficacy. In this work, core-shell electrospun polycaprolactone nanofiber-based membranes, loaded with rifampicin and coated with silver nanoparticles, were developed and characterized. The membranes are composed by randomly oriented nanofibers with a homogeneous diameter, as demonstrated by scanning electron microscopy (SEM). An air-plasma treatment was applied to increase the hydrophilicity of the membranes as confirmed by contact angle measurements. The rifampicin release from untreated and air-plasma treated membranes, evaluated by UV spectrophotometry, displayed a similar and constant over-time release profile, demonstrating that the air-plasma treatment does not degrade the rifampicin, loaded in the core region of the nanofibers. The presence and the distribution of silver nanoparticles on the nanofiber surface were investigated by SEM and Energy Dispersive Spectroscopy. Moreover, SEM imaging demonstrated that the produced membranes possess a good stability over time, in terms of structure maintenance. The developed membranes showed a good biocompatibility towards murine fibroblasts, human osteosarcoma cells and urotheliocytes, reveling the absence of cytotoxic effects. Moreover, doble-functionalized membranes inhibit the growth of *E. coli* and *S. aureus*. Thanks to the possibilities offered by the coaxial electrospinning, the membranes here proposed are promising for several tissue engineering applications.

1. Introduction

The aim of tissue engineering and regenerative medicine is to preserve, recover and improve the lost functions and structures of native tissues and organs caused by pathological conditions, injuries, or iatrogenic damages. This goal can be reached thanks to the use of scaffolds, which are able to mimic the morphology and the macromolecular environment of the native extracellular matrix and can sustain cell adhesion, proliferation, migration and differentiation, therefore promoting tissue regeneration. In this scenario, the electrospinning technique stands as an advantageous and useful approach since it allows to develop nanostructured nanofiber-based matrices, which can mimic the extracellular matrix architecture and structure, possess a large surface area, a highly interconnected porous structure and favors gaseous exchanges [1–3].

The electrospun membranes can be easily functionalized with bioactive molecules and antibacterial compounds whose release can be modulated thanks to the specific porosity, fiber diameter and surface

Abbreviations: DCM, dichloromethane; DMF, *N*,*N*-dimethylformamide; DW, deionized water; EG, ethylene glycol; GBR, Guided Bone Regeneration; nAg, silver nanoparticles; PCL, polycaprolactone; PCL/plasma, plasma treated PCL membranes; PCL/Rif, rifampicin enriched PCL membranes; PCL/Rif/plasma, plasma treated PCL/Rif; PCL/nAg, membranes with nAg; PCL/plasma/nAg, plasma treated PCL/nAg; PCL/Rif/nAg, PCL/Rif with nAg; PCL/Rif/plasma/nAg, plasma treated PCL/Rif/nAg; PDA, polydopamine; Rif, rifampicin; SBF, Simulated Body Fluid; UCs, urotheliocytes.

* Corresponding author at: Department of Life Sciences, University of Trieste, Via Alexander Fleming 31/B, 34127 Trieste, Italy.
E-mail address: dporrelli@units.it (D. Porrelli).
[1] CNR-IOM, Istituto Officina dei Materiali - Consiglio Nazionale delle Ricerche, Strada Statale 14, km 163,5, 34,149 Basovizza, Trieste, Italy.
[2] Department of Life Sciences, University of Trieste, *Via* Licio Giorgieri 5, 34,127, Trieste, Italy.
[3] Department of Life Sciences, University of Trieste, *Via* Alexander Fleming 31/B, 34127, Trieste, Italy.

https://doi.org/10.1016/j.bioadv.2024.214036
Received 20 May 2024; Received in revised form 9 August 2024; Accepted 6 September 2024
Available online 11 September 2024

area, which can be tailored controlling the electrospinning process [4–7]. The ease of preparation and tailoring of nanofibers allow to develop materials for several applications in tissue engineering fields such as bone regeneration [8,9], vascular grafts [10,11], and wound dressings [12,13], but also to develop materials for the controlled and sustained drug release [14], and for cancer treatment [15]. It is possible to produce electrospun nanofibers and membranes with a wide variety of geometries depending on the specific final applications; moreover it is possible to integrate the electrospinning process with other techniques such as electrospraying and solvent casting to properly tailor the mechanical and chemical properties of the nanofibers as well as their solubility [16,17]; and also to apply treatments for the modulation of the membrane stability, such as thermal treatments and cross-linking strategies [18,19].

Exploiting specific needles and combining different strategies it is possible to obtain a huge variety of nanofibers, such as Janus nanofibers, core-shell nanofibers, multilayer membranes, and particles-loaded nanofibers, which can be further modified and tailored to obtain a controlled drug delivery in terms of release kinetics and release stimuli [20]. In particular, core-shell and core-sheath nanofibers (prepared with coaxial needles) can be used for the encapsulation of bioactive molecules, antibiotics or nanostructured systems and water-soluble compound, allowing a sustained and/or prolonged release, reducing the burst release, or enabling the two-stage release of bioactive compounds. Indeed, during the preparation or the modification of the core-shell nanofibers, it is possible to include drugs and bioactive compounds into the core or shell layer, or on the surface of the shell layer, depending on the required release profiles and on the stability of molecules used [7,21–24]. Moreover, modifying the coaxial electrospinning process it is possible to work with complex and unspinnable solvents and molecules to prepare multifunctional nanofibers [25].

The electrospinning process can be further improved combining it with other methods to obtain more complex nanofibers. Edmans et al. included drug-loaded, sub-micrometric polymer spheres in polymer nanofibers to tailor the release of drugs to mucosal epithelia [26]; conversely, Chen et al. explored different strategies based on electrospinning and electrospraying to prepare a material for the modulation of the release of a drug with low water solubility [27]. Moving to more complex architectures and strategies, Zhou et al. exploited the Janus nanofibers structure to load an anticancer drug and a chemical compound to achieve both drug delivery and photothermal therapy [28]; Wang et al. developed trilayer co-axial nanofibers for the fine control of an anticancer drug release and Zhao et al. implemented the trilayer architecture in Janus nanofibers to obtain a three-functionalized material in which two drugs and nano-hydroxyapatite are present and can be delivered to the host tissue in different ways [29]. Other than the architecture and the geometry of the nanofibers, their functionalization is an important aspect to achieve the desired function in particular in terms of controlled and stimulated drug delivery [30,31]; in this context, the possibility to exploit three different regions in a core-shell, Janus or combined core-shell/Janus nanofiber, can give many advantages in terms of drug loading, drug release and tailoring of chemical properties. For example, Janus nanofibers can be chemically modified to be responsive to thermal treatment to enhance the drainage of wound exudate in diabetic wounds [32]; or can be included in a core-shell structure for the controlled delivery of drugs with lower water solubility for application in blood brain barrier [33], or for pH-sensitive drug delivery [34]. In a similar way, Xu et al. designed Janus nanofibers with three different sections, which were loaded with two different drugs in the innermost and middle layer, and with beeswax in the outermost layer in order to achieve an anti-adherent membrane for tendon repair [35].

To produce electrospun membranes, synthetic polymers such as polyvinyl-chloride, polyglycolic acid, polylactic acid, polyethyleneterephthalate, polycaprolactone, polyhydroxyalkanoates, and copolymers are commonly employed with the aim to develop biocompatible medical device with suitable features, such as controlled biodegradability, mechanical properties, and shape memory characteristics to enable tissue regeneration. However, these polymers are generally hydrophobic and do not possess any bioactive features, thus requiring surface treatments and/or the addition of bioactive molecules [5,36,37]. Among synthetic polymers used to produce electrospun nanofibers in the biomedical field, polycaprolactone (PCL) is one of the most noteworthy thanks to its biocompatibility, slow biodegradability (2–4 years), mechanical strength, distinct rheological and viscoelastic properties, and cost-effectiveness, which make it suitable and appealing for long-term implantation. PCL is an aliphatic semicrystalline linear polymer approved by Food and Drug Administration for biomedical uses and already employed for the development of scaffolds for several biomedical purposes such as ureteral regeneration, guided bone regeneration, cardiac tissue regeneration, neuronal regeneration, tendon repair, anticancer treatment, and diabetic wounds healing [3,9,38–40]; and in particular to prepare electrospun core-shell meshes, both in association with natural and synthetic polymers or other nanostructured systems [41–43].

When developing a biomaterial for tissue engineering applications, is important take into consideration the risk of infections that could interest the implant site and might lead to several complications on the structural and functional recovery of the damaged tissue. Therefore, to discourage bacterial infections it is necessary to confer antibacterial properties to the electrospun products by functionalizing the biomaterial with antibacterial agents, such as antibiotics, chemical molecules, metallic nanoparticles or antimicrobial peptides [44–46].

Among the antibiotics, rifampicin (Rif) is widely used because it has a broad-spectrum activity, it is effective against Gram-negative bacteria and Gram-positive, and it is particularly effective against staphylococci, encompassing also the common surgical pathogen *Staphylococcus aureus*. The rifampicin acts on the β-subunit of bacterial RNA polymerase, involving the suppression of the transcription and, as a consequence, also of the bacterial protein synthesis [47–49].

Among metallic nanoparticles, silver nanoparticles have gained remarkable interest for a broad of biomedical applications and there are several research groups that are investigating their applications in different fields such as bone grafts, wound dressings, and vascular grafts [50–54], because of silver nanoparticles wide-spectrum antibacterial efficacy against Gram positive, Gram negative and antibiotic-resistant strains [55]. The silver ions released by the nanoparticles lead to the degradation of the peptidoglycan component of the bacteria cell walls; they inhibit the bacterial protein synthesis binding RNA and interact with DNA blocking cell replication; moreover, silver ions cause oxidative stress, leading to cytoplasmic damage and to the killing of bacterial cells [56].

An interesting aspect of the antibacterial compounds is that they can be used in various combinations in order to exploit their activities in a synergistic way, as demonstrated by Deng and colleagues [57] and Vazquez-Muñoz and colleagues [58], whose work demonstrated that silver nanoparticle and antibiotics can enhance each other effects by interacting with bacterial cells.

Inspired by the opportunities offered by coaxial electrospinning and by the recent findings on the synergistic use of antibacterial compounds, the work here reported describes the development of coaxial electrospun membranes based on core-shell polycaprolactone nanofibers. The nanofibers are constituted by a core loaded with rifampicin and a shell functionalized with polydopamine and coated with silver nanoparticles. The obtained material was characterized in order to analyze its morphology, test its stability and evaluate the release of the antibacterial compounds. The material was also tested on fibroblasts, osteoblasts and urotheliocytes in order to assess its biocompatibility and suitability for different tissue engineering applications, and the antibacterial properties were verified towards *Staphylococcus aureus* and *Escherichia coli*.

2. Materials and methods

2.1. Materials

Polycaprolactone (PCL, Mw = 80,000), dichloromethane (DCM), *N*, *N*-dimethylformamide (DMF), methanol, chloroform, silver nitrate, dopamine hydrochloride powder, Tris-base and phosphate buffered saline (PBS) were purchased from Merck (St. Louis, MO, USA). Glass syringes (with an inner diameter of 14.6 mm), three-layers coaxial needle, and coaxial kit were acquired from Linari NanoTech (Pisa, Italy). The KDS-100-CE syringe pump was purchased from KD Scientific (Holliston, MA, USA). Rifampicin (Rif) was purchased from EMD Millipore Corp (Burlington, MA, USA). The D-ES30PN-20 W potential generator was purchased from Gamma High Voltage Research Inc. (Ormond Beach, FL, USA). Recombinant Trypsin−EDTA 1×, penicillin/streptomycin 100×, L-glutamine 100×, fetal bovine serum (FBS), and and Dulbecco's modified Eagle's medium, Low and High Glucose (DMEM-LG, DMEM-HG) were purchased from Euroclone (Milan, Italy). All other chemicals were of analytical grade and were purchase from Merck (St. Louis, MO, USA).

2.2. Preparation of core-shell membranes

Core-shell membranes (PCL) were obtained modifying protocols previously published by Gruppuso *et al* [2]. To produce the core of the PCL core-shell membranes, PCL 12 % *w/v* was dissolved in a DCM/DMF mixture (volume ratio 7:3), first preparing the solution of PCL in DCM and, subsequently, adding DMF to the solution. In the case of Rif-loaded membranes (PCL/Rif), the rifampicin 0.1 % *w/v* was solubilized in DMF and, afterwards, added to PCL solution in DCM. For the preparation of the shell solution, PCL 15 % w/v was dissolved in a chloroform/methanol mixture (volume ratio 5:1), first making the solution of PCL in chloroform and, following, adding methanol to the solution. Electrospun core-shell membranes were obtained through the following experimental set-up: time of the process, 30 min; voltages, 30 kV; core solution flow rate, 1 mL/h; shell solution flow rate, 3 mL/h; needle-to-collector distance, 30 cm; inner spinneret diameter, 21G; outer spinneret diameter, 15 G; negative pole to the target.

2.3. In situ synthesis of silver nanoparticles

The coating of silver nanoparticles (nAg) was prepared by an *in-situ* reduction of silver ions. Two solutions, of dopamine hydrochloride and silver nitrate ($AgNO_3$), were separately prepared, adapting a protocols published by Son et al. [59]. Dopamine hydrochloride 0.2 % *w/v* was solubilized in deionized water with Tris-base 10 mM and stirred overnight to reduce amount of aggregation of polydopamine. The solution pH was adjusted to 8.5 with the aim to allow the self-polymerization of dopamine [60]. Simultaneously, $AgNO_3$ 2 mM was dissolved in deionized water. Once obtained both solutions, they were mixed (volume ratio 1:1), in order to obtain a final concentration of dopamine hydrochloride of 0.1 % *w/v* and silver nitrate of 1 mM. In the next step, the core-shell matrices were immersed into coating solution at room temperature for 6 h. Lastly, to remove the excess amount of coating solution, the core-shell membranes were rinsed with deionized water 5 times and subsequently air dried. Silver nanoparticles coated membranes without or with rifampicin are indicated as PCL/nAg and PCL/Rif/nAg respectively.

2.4. Air-plasma treatment

An air-plasma cleaning process was used to increase the hydrophilicity of the membranes. The air-plasma treatment was performed using a PDC-32G plasma cleaner (Harrick Plasma, Ithaca, NY, USA) set at low power (6.8 W), at a pressure of 0.1 mTorr for 30 s. Membranes treated with the air-plasma cleaning process were here named as PCL/plasma, PCL/Rif/plasma, PCL/plasma/nAg and PCL/Rif/plasma/nAg.

2.5. Membrane morphological analysis by scanning electron microscopy (SEM) and energy dispersive spectroscopy (EDS)

To investigate the morphology and the structure of the nanofibers, membranes samples were placed on aluminum stubs covered with carbon double-side adhesive tape and, subsequently, carbon coated using pulsed carbon rod evaporation with a Quorum Q150T ES plus sputter coater (Quorum Technologies Ltd., Lewes, UK). Samples were analyzed with a Gemini300 Scanning Electron Microscope (Zeiss, Oberkochen, Germany) working with the secondary electrons and backscattered electrons, at 5 mm of working distance and using an acceleration voltage of 5 kV. The images of nAg were obtained reversing the contrast of images collected with backscattered electrons, thus obtaining a TEM (Transmission Electron Microscopy)-like imaging. Microanalysis was performed with an XFlash Detector 610 M EDS probe (Bruker, Billerica, MA, USA), using a magnification of 500×, a working distance of 8.5 mm, an acceleration voltage of 10 kV and an acquisition time of 200 s; three spectra were collected for each sample. Fibers diameters were obtained using Fiji software, randomly choosing 50 fibers from each membrane.

2.6. Contact angle and surface energies analyses

The wettability of the membrane was evaluated thanks to measurement of the contact angle, through the sessile drop method. For each condition, 6 samples of membranes were analyzed. Contact angle was measured on images acquired with an optical microscope Leica MZ16 (Leica, Wetzlar, Germany) equipped with a 45° titled mirror and a digital camera Leica DFC 320, through which was possible to display the profile of the liquid drop on the membrane sample. The membranes behavior was evaluated in the presence of 4 μL of liquid deionized water (DW) and DMEM and the images were acquired after 30 s to allow drop stabilization. Image Pro-Plus Suite software (Meyer Instruments Inc., Houston, TX, USA) was used to process the images and to measure the contact angle. Surface energies were assessed using the Owes-Wendt method [61] adjusted by Ren et al. [62] and Can-Herrera et al. [63]. In addition to the water contact angle, ethylene glycol (EG) contact angle (measure placing 4 μL of liquid on the samples) was used to calculate both the surface energy (γ_s) polar/hydrophilic (γ_s^p) and dispersive/hydrophobic (γ_s^d) components.

2.7. Simulated body fluid preparation and evaluation of membranes aging

Membranes aging was carried out by samples immersion in Simulated Body Fluid (SBF) at 37 °C. The SBF was prepared by solubilizing NaCl, $NaHCO_3$, KCl, K_2HPO_4, $MgCl_2{\cdot}6H_2O$, $CaCl_2$, and Na_2SO_4 in deionized water and buffering the solution at pH 7.4 with tris(hydroxymethyl)aminomethane $(CH_2OH)_3CNH_2$ and 1 M HCl at 36.5 °C [64]. The effects of the SBF aging on the membranes structural stability were evaluated after 8 weeks. Samples were soaked in 500 μL of SBF, which was changed every week.

2.8. Rifampicin release

The release of rifampicin from treated and untreated PCL/Rif membranes was assessed by means of UV spectrophotometry at wavelength of 237 nm (Ultraspec 2100 pro, Amersham Biosciences, Amersham, UK). To estimate the release of rifampicin, membranes samples (disks of 12.7 mm diameter) were soaked in 1 mL of saline phosphate buffer (PBS) in 24-well plates. After 1,4, 24, 48, 72 h, and 1 week. 800 μL of solution was taken from each well for absorbance evaluation. The release solution was substituted with fresh PBS at each time point. Between measurements, the plate was incubated at 37 °C in the dark.

2.9. Silver adsorption and release evaluation with inductively coupled plasma−mass spectrometry

To assess the adsorption and the release of silver from core-shell matrices, ten PCL not treated and PCL air-plasma membrane samples (diameter, 6 mm) were coated with 200 μL of the solution containing silver nitrate and polydopamine hydrochloride, for 6 h at room temperature in dark conditions. The release of the silver from core-shell matrices was performed by immersion of the membrane samples in 500 μL of PBS at 37 °C in 48-well plate, and evaluated at 1, 4, 24, 48 h and 1 week in dark condition. At each time point, the supernatant was collected from each well and stored for the release evaluation. Membrane samples were dissolved in 500 μL of concentrated nitric acid (67–69 % *v*/v, Normatom, VWR, Milan, Italy) and sonicated 15 min at 50 °C to promote complete dissolution. The Ag concentration was determined by Inductively Coupled Plasma – Mass Spectrometry (ICP – MS) using a NexION 350× Spectrometer (PerkinElmer, Waltham, MA, USA) equipped with an ESI SC Autosampler. To minimise cell-formed polyatomic ion interferences, the analysis was carried out in KED mode (Kinetic Energy Discrimination) with a very high purity helium flow of 4.8 mL/min. The instrument was calibrated by analysing standard solutions ranging between 0.5 and 100 μg/L prepared by dilution of a multistandard solution of 10 mg/L for ICP analysis (Periodic Table MIX 1, TraceCERT Merck, St. Louis, MO, USA). The ICP-MS calibration curve was linear ($R^2 = 0.999$; selected ion mass: 107 in the concentration range. To minimise potential matrix effects, the internal standard method was used. For this purpose, a solution of Y (89 spike of 50 μg/L) was prepared from a standard solution at 1000 mg/L (Yttrium Standard for ICP, TraceCERT Merck, St. Louis, MO, USA). For the ICP analysis, 1 mL of internal standard solution (Y at 500 μg/L) was added to the membrane samples, and the final volume was set to 10 mL. Whereas, for the quantification of silver released from membranes, the obtained samples (500 μL) were diluted to a final volume of 5 mL, after adding 100 μL of HNO_3 and 500 μL of internal standard. Accuracy was assessed by analysing two quality control solutions at 1 μg/L and 10 μg/L, prepared from a multistandard solution different from the one used for instrument calibration (Multielement quality control standard for ICP, VWR Chemicals, Milan, Italy). The limit of detection (LOD) was 0.05 μg/L, and the measurement precision as repeatability (RSD%) for the analysis was <3 %.

2.10. Cell culture

Murine fibroblasts (NIH/3 T3, ATCC CRL-1658, ATCC, Manassas, VA, USA) and osteosarcoma-derived human osteoblasts (MG-63, ATCC code: CRL-1427) were cultured in DMEM-HG supplemented with FBS 10 %, L-glutamine 2 mM, penicillin 100 U/mL and streptomycin 0.1 mg/mL at 5 % pCO_2 and at 37 °C. Human urothelial bladder carcinoma cells (UCs - line 647-V, DSMZ, Braunschweig, Germany) were cultured in DMEM-LG supplemented as the DMEM-HG. Cell lines were passed three times a week or when the confluence level was estimated at about 70–80 % of the available culture space.

2.11. Proliferation assay

Membranes were cut in disc samples (6 mm in diameters) and were sterilized with UV irradiation using a G30T8 UV-C germicidal lamp (wavelength: 253.7 nm; power: 13.4 W, Sankyo Denki, Hiratsuka, Japan) for 15 min per side. NIH-3 T3, MG-63 and UCs cells were suspended in complete medium at a concentration of 5×10^3 cells/well, seeded in 24-well cell culture plates (1 mL for each well) and then incubated at 37 °C with 5 % pCO_2. After 4 h of incubation, disc samples were added to the cells. Cells grown in the absence of samples were used as proliferation control, while empty wells with the culture medium only were used as blanks. Cell proliferation was evaluated after 1, 3, 6 and 8 days using the Resazurin Cell Viability Assay Kit (Sigma-Aldrich, St. Louis, MO, USA), by testing five samples for each type of membrane. At each time point, the medium was removed from the culture wells and 500 μL of Resazurin (diluted 1/30 in culture medium) were added to each well. After 4 h of incubation, 200 μL of the reacted medium were collected from each well and placed in a 96 well black plate for the fluorescence analysis. After the removal of reacted medium, cell culture wells were washed twice with 1 mL of PBS and then 1 mL of fresh culture medium was added to each well. The fluorescence was evaluated using the GloMax Multi+ Detection System spectrofluorometer (Promega, Madison, WI, USA) with an excitation wavelength of 525 nm and an emission wavelength in the range 580–640 nm. Cell proliferation rate was calculated as the ration between the fluorescence reads at the different time points to the fluorescence reads of day 1, after the subtraction of the blank.

2.12. Bacterial strains culture

Escherichia coli (*E. coli* – ATCC 25923) and *Staphylococcus aureus* (*S. aureus* – ATCC 25922) were plated on agarized Mueller-Hinton (MHA; Oxoid S.p.A., Milan, Italy) from a glycerol stored at −80 °C and subsequently bacteria were grown overnight at 37 °C. To grow liquid culture, some bacterial colonies were taken and dispersed in 4 mL of MH medium. Bacterial inoculum was incubated over-night at 37 °C with shacking (120 rpm). The day after, 300 μL of each bacterial culture were added to 10 mL of fresh MH medium and then incubated at 37 °C and 120 rpm for about 90 min until bacterial culture reached an optical density measured at wavelength of 600 nm (OD_{600}) of 0.3 measured by spectrophotometry (Ultraspec 2100 pro, Amersham Bioscience). The reference values, empirically calculated, used to calculate the bacterial concentration (CFU/mL) starting from the OD_{600} were OD_{600} 0.31: 4.6×10^7 CFU/mL for *E. coli* and OD_{600} 0.1: 5×10^8 CFU/mL for *S. aureus*, respectively.

2.13. Assessment of antibacterial properties of the membranes

Membranes samples (disks of 6 mm diameter) were sterilized under UV rays for 30 min, then placed on a 24-well plate. Bacteria from a mid-log phase culture were diluted in MH medium to achieve a final concentration of 2.5×10^5 CFU/mL and used to evaluate the capability of materials to inhibit bacterial proliferation. 4 samples for each type of membranes (PCL, PCL/nAg, PCL/Rif, and PCL/Rif/nAg) were put in the wells of a 24-wells plate, then 380 μL of bacterial suspension were added to the wells to cover the membrane disks. Meanwhile, 380 μL of MH medium only were used as a negative growth control and 380 μL of bacterial culture without membranes were used as a positive growth control. The samples were incubated at 37 °C over-night and after 18 h from the plate was firstly checked by naked eye for medium turbidity. After that, to better evaluate the bacterial growth in the presence of the material, 200 μL of bacterial suspension were collected from each well, added to 800 μL of MH medium and subsequently used for absorbance measurements at 600 nm. The inhibition of bacterial growth was evaluated comparing the absorbance of the bacterial suspensions growing in the presence or in the absence of the membranes. The OD measures were used also to calculate the concentration of the bacterial cells, as CFU/mL, using predictive models as reported by Guagnini et al. [65].

3. Results

3.1. Electrospun core-shell fibers morphology

Electrospun core-shell PCL (PCL, Fig. 1A) and Rif-loaded fibers (PCL/Rif, Fig. 1B) were developed by adapting the protocols previously published by Gruppuso *et al* [2]. Both types of core-shell fiber were characterized by randomly oriented and packed fibers and a homogeneous and dense fibrous matrix. Moreover, the fibers did not show any superficial defects, such as beads. In addition, the introduction of the

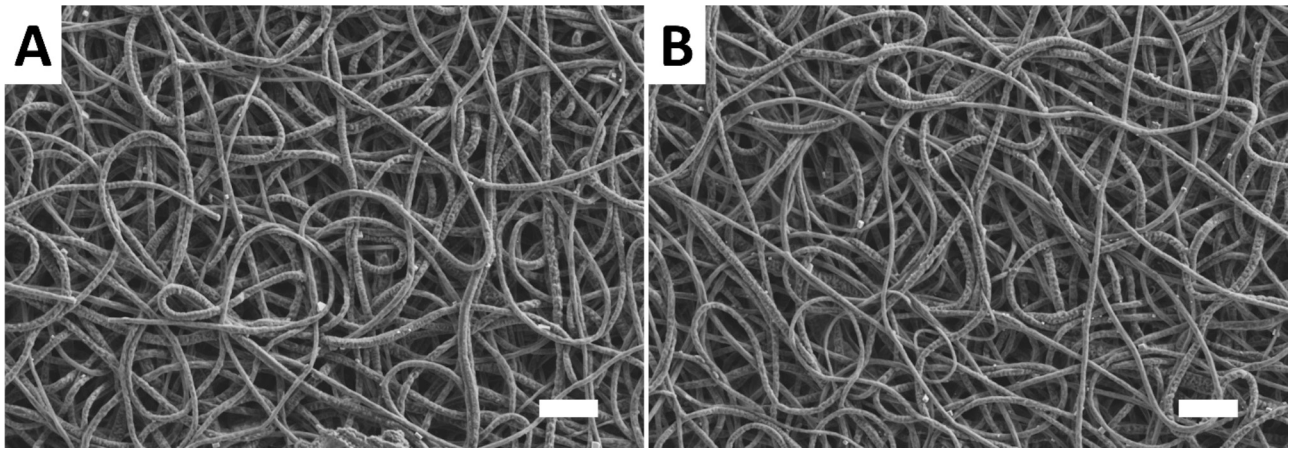

Fig. 1. SEM micrographs of PCL membranes. PCL (A), PCL/Rif (B) membranes. Scale bar (white) is 10 μm.

rifampicin in the core did not affect the fibers diameter and their morphology. In details, the average diameter of the PCL core-shell nanofibers was 2.14 ± 0.64 μm, while that of the Rif-loaded core-shell nanofibers was 1.94 ± 0.82 μm.

3.2. *In situ synthesis of silver nanoparticles on Core-Shell membranes*

In order to functionalize the shell layer of the core-shell nanofibers, the membranes were immersed in a solution of dopamine hydrochloride and silver nitrate with the aim to allow the *in-situ* synthesis of silver nanoparticles on the surface of the fibers. The protocol of the *in-situ* reduction of silver nanoparticles on electrospun matrices was adapted from Son *et al* [59]. When the membranes were immersed in the coating solution, dopamine self-polymerized forming polydopamine (PDA). The oxidation reaction caused the reduction of the silver (Ag^{1+}) into metallic silver (Ag^{0}) allowing the synthesis of the silver nanoparticles (nAg) on the core-shell fibers. The presence and the distribution of nAg were analyzed by SEM and EDS analyses (Fig. 2). In detail, the deposition of silver nanoparticles was homogeneous in both PCL/Rif and PCL/Rif/plasma membranes as can be appreciated in Fig. 2A-B and 2D-E, where the nAg are shown as black dots, since the images were collected using the backscattered electrons obtaining a TEM-like image. In the Supplementary Material, Fig. S1 and S2 report further images of PCL/Rif/nAg and PCL/Rif/plasma/nAg respectively. The EDS spectra of PCL/Rif/nAg and PCL/Rif/plasma/nAg membranes are reported in Fig. 2C and F and confirmed the presence of silver on the membranes.

To test if the PDA was necessary for the *in situ* synthesis of nAg, PCL/Rif and PCL/Rif/plasma membranes were placed in the solution of $AgNO_3$ without PDA. The EDS spectra reported in Fig. S3 show that in case of PCL/Rif membranes silver was not detectable, while for PCL/Rif/plasma membranes a weak signal of silver was detected although the presence of nAg was not detectable in SEM imaging (data not shown).

3.3. *Evaluation of wettability, contact angle, and surface energy of electrospun membranes*

The wettability of PCL and Rif-loaded membranes (Fig. 3) was analyzed through contact angle measurements using deionized water (DW). Both plasma-treated and not-treated membranes were tested with the aim to evaluate the effectiveness of the air-plasma treatment in

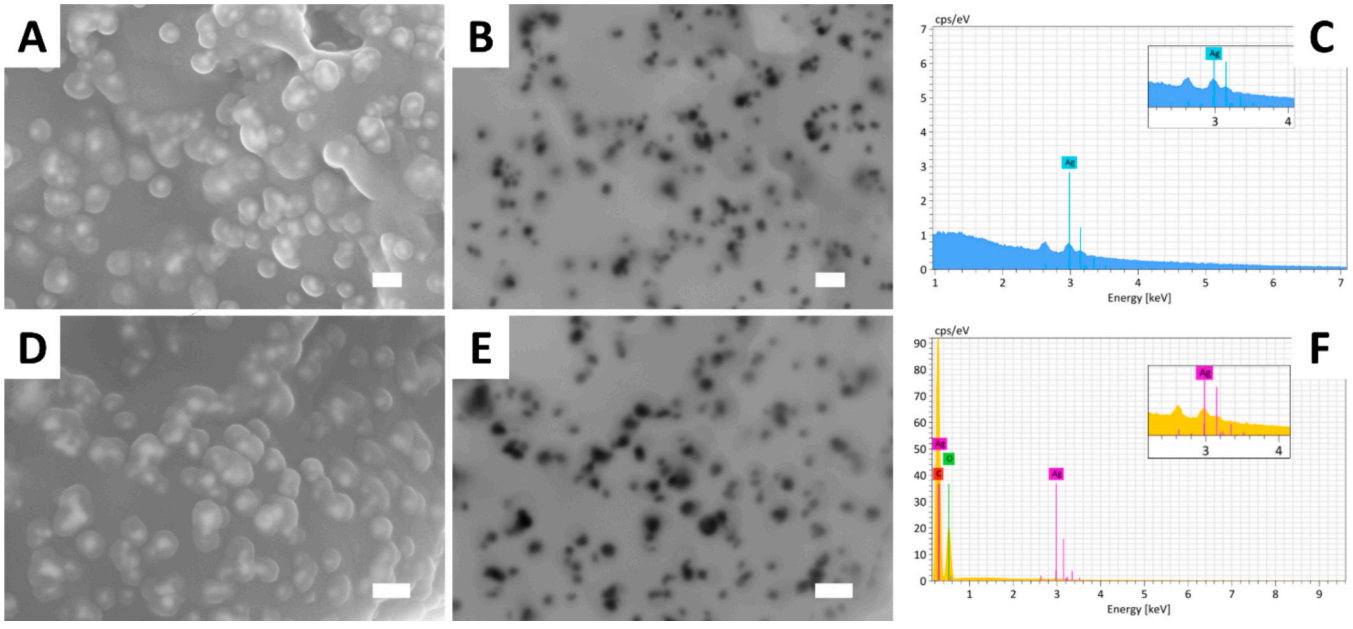

Fig. 2. Evaluation of the presence of the silver nanoparticles. SEM and TEM-like images of the deposition of silver nanoparticles on PCL/Rif membrane (A, B) and PCL/Rif/plasma membrane (D, E). Scale bar is 400 nm. EDS spectra of PCL/Rif/nAg membrane (C) and PCL/Rif/plasma/nAg membrane (F).

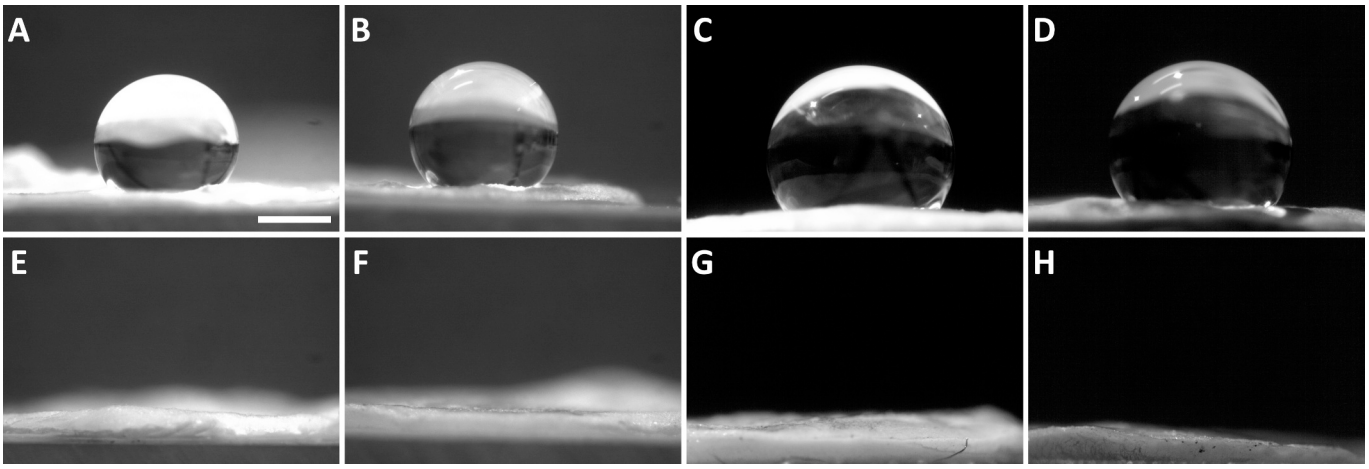

Fig. 3. Membranes wettability. Contact angle analysis of PCL and PCL/plasma membranes (A, E), PCL/Rif and PCL/Rif/plasma membranes (B, F), PCL/nAg and PCL/plasma/nAg membranes (C, G), and PCL/Rif/nAg and PCL/Rif/plasma/nAg (D, H). Scale bar is 1 mm.

increasing the membranes hydrophilicity. Both in the case of not treated PCL and PCL/Rif electrospun membranes (Fig. 3A, C), contact angle measurements confirmed the hydrophobicity of the polymer. On the other hand, the membranes that were subjected to the air-plasma treatment, showed a total wettability indicating the effectiveness of this type of treatment in modifying the surface properties of PCL-based membranes (Fig. 3E-H). Thereafter, the surface free energy of treated and not-treated membranes was calculated according to the Owens-Wendt method. Contact angle values and surface energy values are reported in Table 1. The hydrophobicity of not-treated PCL-based membranes was confirmed by observing the high contact angle values (>90°) and the low values of polar component of the surface energy. Meanwhile, the treated membranes showed an increment of surface energy polar component values confirming the effectiveness of the air-plasma treatment towards the membranes.

3.4. Rifampicin cumulative release kinetics

With the aim to estimate the release of rifampicin from the core of the core-shell fibers, untreated and treated Rif-loaded membranes were incubated at 37 °C in PBS, at 1, 4, 24, 48 h and 1 week. The absorbance of released rifampicin was measured by UV–visible spectrophotometry and its amount subsequently was quantified using the Lambert−Beer equation, knowing that its ε_{237} nm is equal to 33,200 (as calculated from a calibration curve), and normalized on 1 mg of membrane. The Fig. 4 display the rifampicin release profiles from core-shell matrices. In the first 4 h, untreated Rif-loaded and treated Rif-loaded membranes showed a very comparable release profile. In detail, after 4 h of incubation in PBS, both type of membranes released about 30 % of the Rif. After 24 h of incubation in PBS, the amount of rifampicin released was slightly higher than the amount noted for both types of membranes at 4 h. In detail, at 24 h of incubation, the untreated Rif-loaded membranes allowed a release up to 37.2 % of rifampicin included within the core, meanwhile the Rif-loaded air-plasma treated membranes enabled a release of 35.7 % and, therefore, slightly less than untreated membranes. Lastly, from 24 h up to 1 week, both treated and not-treated PCL/Rif membranes slightly increased the release of rifampicin from the fibers as well as constant release over time. Specifically, at 1 week of incubation in PBS, the untreated PCL/Rif fibers released about 41.8 % of the total rifampicin while the air-plasma treated PCL/Rif fibers released the 39 % of the total rifampicin, without any statistically significant differences for both membranes. The almost identical rifampicin release profiles and kinetics between untreated and air-plasma treated membranes confirmed that loading the rifampicin in the core region of the fibers

Table 1
Contact angle values and surface energy values of core-shell PCL-based membranes.

Membranes	DW contact angle (°)	EG contact angle (°)	γ_{ds} [mJ/m^2]	γ_{ps} [mJ/m^2]	γ_s (tot) [mJ/m^2]
PCL	123 ± 3	0	79.5 ± 0.1	12.3 ± 1.5	91.8 ± 0.1
PCL/Plasma	0	0	79.5 ± 0.1	19.0 ± 0.1	98.5 ± 0.1
PCL/Rif	125 ± 6	0	79.5 ± 0.1	13.3 ± 3.3	92.8 ± 0.1
PCL/Rif/plasma	0	0	79.5 ± 0.1	19.0 ± 0.1	98.5 ± 0.1
PCL/nAg	115 ± 9	0	79.5 ± 0.1	8.8 ± 3.8	88.3 ± 0.1
PCL/plasma/nAg	0	0	79.5 ± 0.1	19.0 ± 0.1	98.5 ± 0.1
PCL/Rif/nAg	121 ± 9	0	79.5 ± 0.1	11.6 ± 4.6	91.1 ± 0.1
PCL/Rif/plasma/nAg	0	0	79.5 ± 0.1	19.0 ± 0.1	98.5 ± 0.1

DW: deionized water; EG: ethylene glycol; nAg: silver nanoparticles; PCL: polycaprolactone; Rif: rifampicin; γ_{ds}: dispersive component of surface energy; γ_{ps}: polar component of surface energy; γ_s: surface energy.

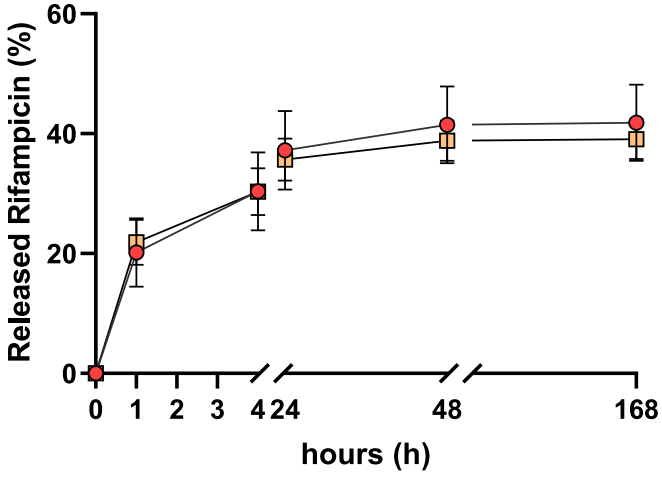

Fig. 4. Release kinetics of rifampicin from membranes. Rifampicin release, reported as the percentage of cumulative release over the total rifampicin contained within the membranes, from PCL/Rif membranes (red circle) and PCL/Rif/plasma membranes (yellow square). No statistically significant difference was observed between the two groups. Error bars represent the standard deviation calculated on the mean on 10 samples.

shielded the antibiotic from the degrading effects of the air-plasma treatment.

3.5. Silver cumulative release kinetics

With the objective to assess the silver release from the shell layer of the core-shell fiber, PCL/Rif/plasma/nAg samples were incubated at 37 °C in PBS, at 1, 4, 24, 48 h and 1 week. The amount of the silver release was evaluated by means of Inductively Coupled Plasma - Mass Spectrometry (ICP-MS). The Fig. 5 show the silver release profiles from core-shell matrices. In the first 4 h, PCL/Rif/plasma/nAg showed a silver burst release. In detail, after 4 h of incubation in PBS, the amount of released silver was about 32 %, indicating an immediate availability of the silver to be potentially addressed towards bacteria pathogens. After 24 h of incubation in PBS the release slowed down, since PCL/Rif/plasma/nAg released the 47 % of the total silver content. Then, after 1 week of similar incubation, the release was 57 %. This guaranteed the remaining of an amount equal to 43 % of residual silver on the membranes.

3.6. Stability characterization of electrospun PCL-based membranes

To evaluate the effects of the aging of membranes under physiological-like conditions, the membranes were immersed in SBF for 8 weeks at 37 °C. The effects of the membranes aging on the fiber morphology and structure are appreciable in Fig. 6 (PCL/Rif/plasma, A; PCL/plasma/nAg, B; PCL/Rif/plasma/nAg, C). In all cases, the membranes did not display any morphological alteration affecting the nanofibers after the incubation, with the exception of a slight increase in the diameter of the nanofibers coated with nAg, which could be due to the swelling of the nanofibers during the procedures of nAg synthesis.

The Fig. 7 reports the SEM images and TEM-like images collected with backscattered electrons for PCL/plasma/nAg (A and B respectively) and PCL/Rif/plasma/nAg (C and D respectively). The images showed that in both cases, the silver nanoparticles are homogeneously distributed on the fiber surface also after 8 weeks of immersion in SBF.

In the Supplementary Material, Fig. S4 and S5 report further images of PCL/Rif/nAg and PCL/Rif/plasma/nAg respectively.

The analysis of the nAg average dimension and distribution is reported in Fig. 8. A different behavior can be appreciated between the two types of membranes: nAg on non-treated membranes are smaller with respect to the treated ones and after the membrane aging the average diameter slightly increase; while for plasma treated membranes the initial average diameter is slightly higher and varies less after the membrane aging.

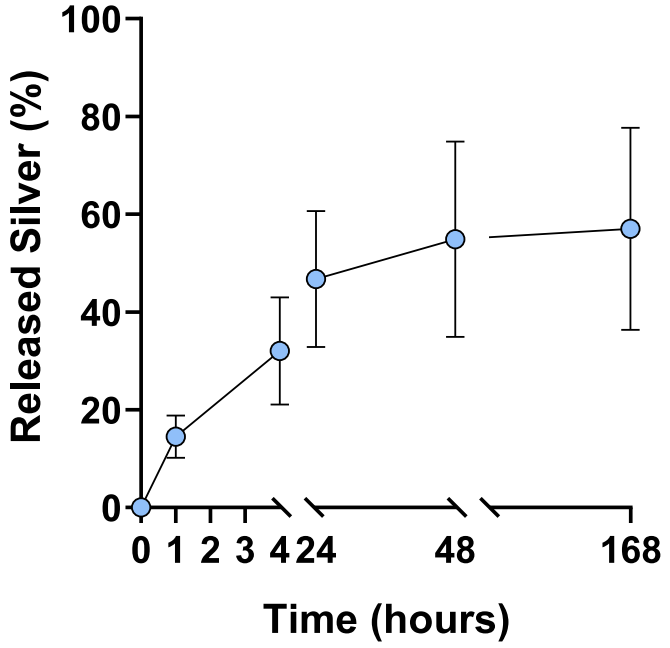

Fig. 5. Silver release kinetics. Silver release kinetic of the PCL/Rif/plasma/nAg membranes, reported as the percentage of cumulative release over the total silver deposited on the membranes. Error bars represent the standard deviation calculated on the mean on 10 samples.

3.7. Biocompatibility of electrospun membranes

To examine the possible cytotoxic effects of the rifampicin released and of the silver nanoparticles or their synergic effect, the biocompatibility of the membranes was tested towards murine fibroblasts NIH/3 T3, human osteoblasts MG-63 and human urotheliocytes UCs, which were cultured in the presence of the biomaterial up to 8 days. As growth control for all types of membranes, untreated cells were used and the proliferation was normalized on day 1 with the aim to calculate the proliferation rate. For the sake of clarity, Fig. 9 shows the proliferation rate of the three types of cells in the presence of PCL/Rif/plasma/nAg, compared with the control of cell proliferation. In the case of NIH/3 T3, PCL membranes allowed a remarkable increase of cell proliferation rate between the first day and sixth day. However, starting from sixth up to eighth day it is possible to observe a slowdown in growth for all type of membranes. This was most probably not due to a potential cytotoxic effect of the rifampicin or silver nanoparticles but rather to the cell confluence which slowed cell metabolism altering the resazurin fluorescence signal. Regarding MG-63 cells the proliferation rate was similar than that observed by NIH/3 T3. Moreover, the proliferation rate was constant until up eighth day of culture, further confirming the absence of any cytotoxic effects.

UCs showed a considerable proliferation rate indicating that the rifampicin contained in the inner moiety of the fibers, together with the silver nanoparticles on the shell, did not affect the cell viability. There were no statistically significant differences among all tested cell lines. Therefore, all the matrices tested displayed good biocompatibility, with no toxic effects deriving from the released rifampicin and silver nanoparticles.

In the Supplementary Materials, the proliferation rate of the three tested cell types, in the presence of all the materials prepared, is reported. The proliferation rate of cells grown in the presence of PCL/Rif/plasma/nAg was compared with the membranes with Rif or nAg only, and also with the membranes not treated with air-plasma treatment in order to determine the potential toxicity of the single components or of the possible presence of biproducts. Fibroblasts (Fig. S6) and osteoblast (Fig. S7) displayed the same trend, reaching a plateau. Conversely, the plateau was not reached in the case of urotheliocytes in the presence of any of the tested materials (Fig. S8).

3.8. Antibacterial properties of PCL-based core-shell fibers

The potential of PCL-based membranes to prevent the occurrence of bacterial growth was assessed using reference strains of clinically relevant pathogens, namely, *E. coli* and *S. aureus*. The bacterial growth in the presence of air-plasma treated membranes was assessed measuring the turbidity of the bacterial culture at 600 nm and compared with that of a control culture of bacteria growing in the absence of the biomaterial (Fig. 10, the data are also reported as CFU/mL in Fig. S9). Fig. 10A shows the inhibitory effect on the bacterial growth of the PCL-based membranes that have not undergone any aging process in SBF. In detail, the treated PCL/plasma/nAg showed a good antimicrobial effectiveness against *E. coli* while towards *S. aureus,* the same membranes did not show any inhibitory effect. On the other hands, the PCL/Rif/plasma membranes discouraged the bacterial growth of *S. aureus,* but did not exert any effect against *E. coli.* Therefore, PCL/Rif/plasma/nAg membranes were examined, with the expectation to dissuade the

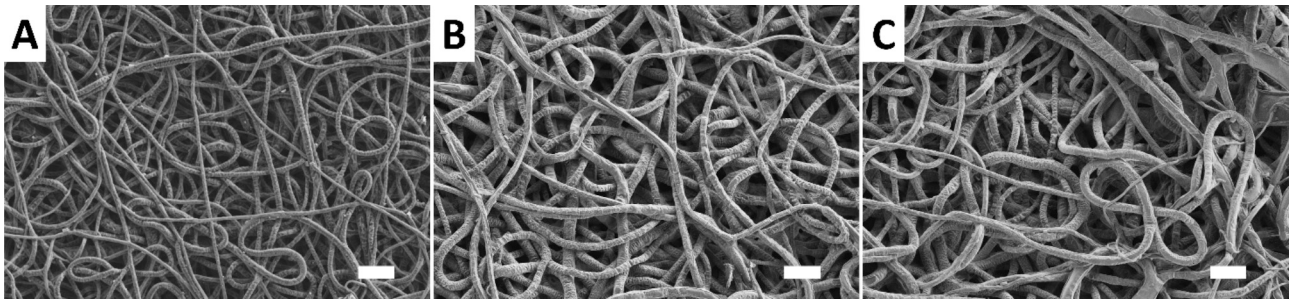

Fig. 6. SEM imaging at different magnification of the morphology of the PCL/Rif/plasma (A), PCL/plasma/nAg (B) and PCL/Rif/plasma/nAg (C). The scale bar (white, panel A) is 10 μm.

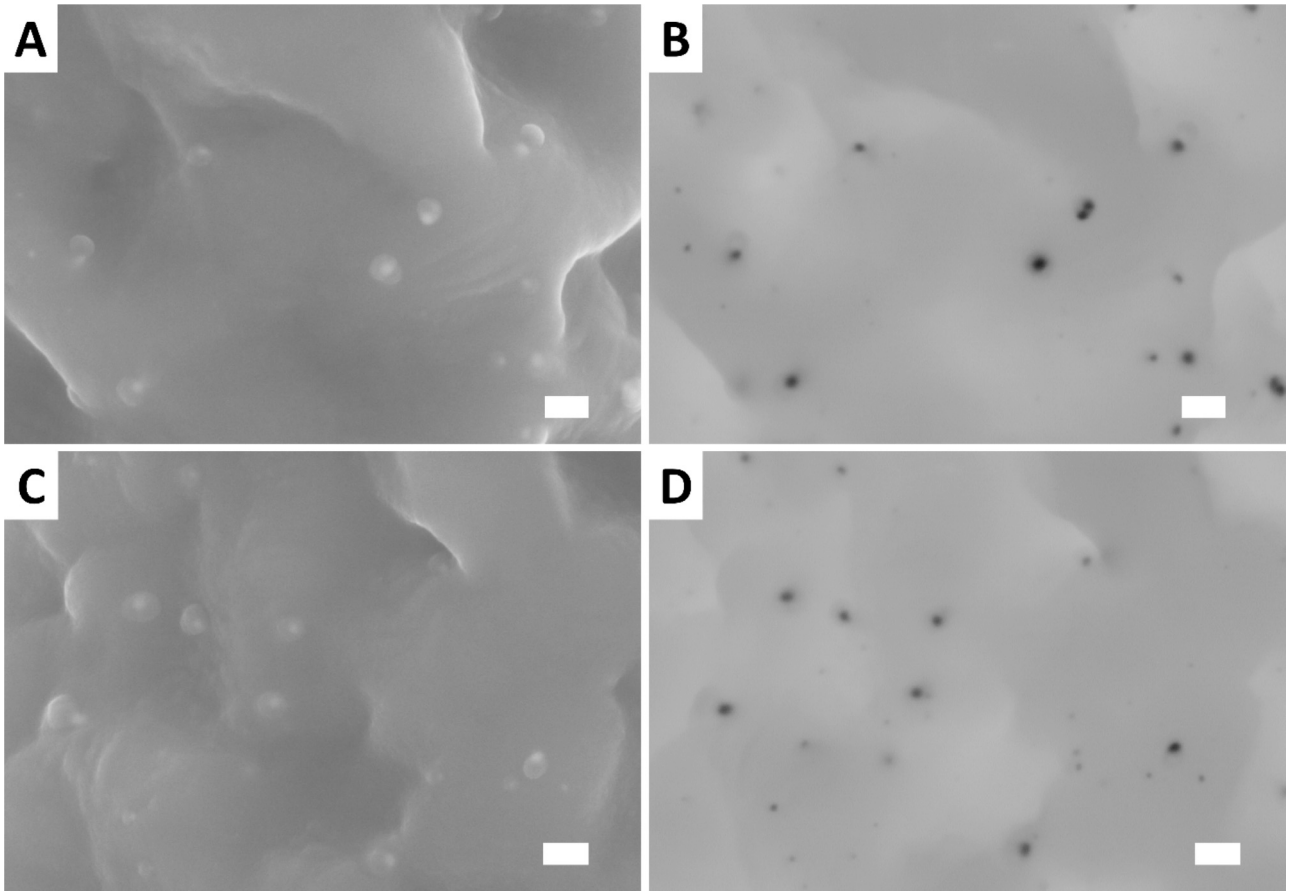

Fig. 7. SEM images and TEM-like images, obtained using the backscattered electrons in SEM analysis, of nAg on aged PCL/Rif/nAg (A, B) and PCL/Rif/plasma/nAg (C, D). The scale bar is 100 nm.

proliferation of both the tested bacterial strain. As supposed, these of membranes strongly inhibited *S. aureus* and *E. coli* growth. This is due by the synergic effect of rifampicin released from the core and the silver nanoparticles release from the shell. PCL/plasma membranes, used to exclude any impairment of bacterial growth due to the PCL or to the plasma treatment, did not display any antibacterial effect against tested bacterial strains.

Then with the aim to verify the antibacterial efficacy over time, the membranes were aged in SBF for 1 week. The Fig. 10B showed the potential inhibitory effect of the PCL-based membranes aged in SBF. The 1-week aging in SBF influenced the antibacterial efficacy of the functionalized membranes, both in the case of *E. coli* and *S. aureus*. However, a slight inhibitory activity was retained with respect to the control of PCL solely. Indeed, *E. coli* growth was partially affected in the presence of the PCL/plasma/nAg and PCL/Rif/plasma/nAg mats. On the other hand, *S. aureus* was in part inhibited by all the functionalized matrices, namely PCL/plasma/nAg, PCL/Rif/plasma, and the combined PCL/Rif/plasma/nAg membranes.

4. Discussion

This work describes the production and characterization of PCL membranes based on core-shell fibers implemented with antibacterial compounds for tissue engineering applications. PCL is in the spotlight for different tissue engineering and regenerative medicine applications (bone, skin, cardiac tissue, meniscus and retinal degeneration) [66–69]. The protocol here used for the preparation of reproducible and handleable core-shell membranes was adapted from the study previous published of Gruppuso *et al* [2]. The process parameters were tuned with to obtain stable and easy to handle membranes characterized by a dense

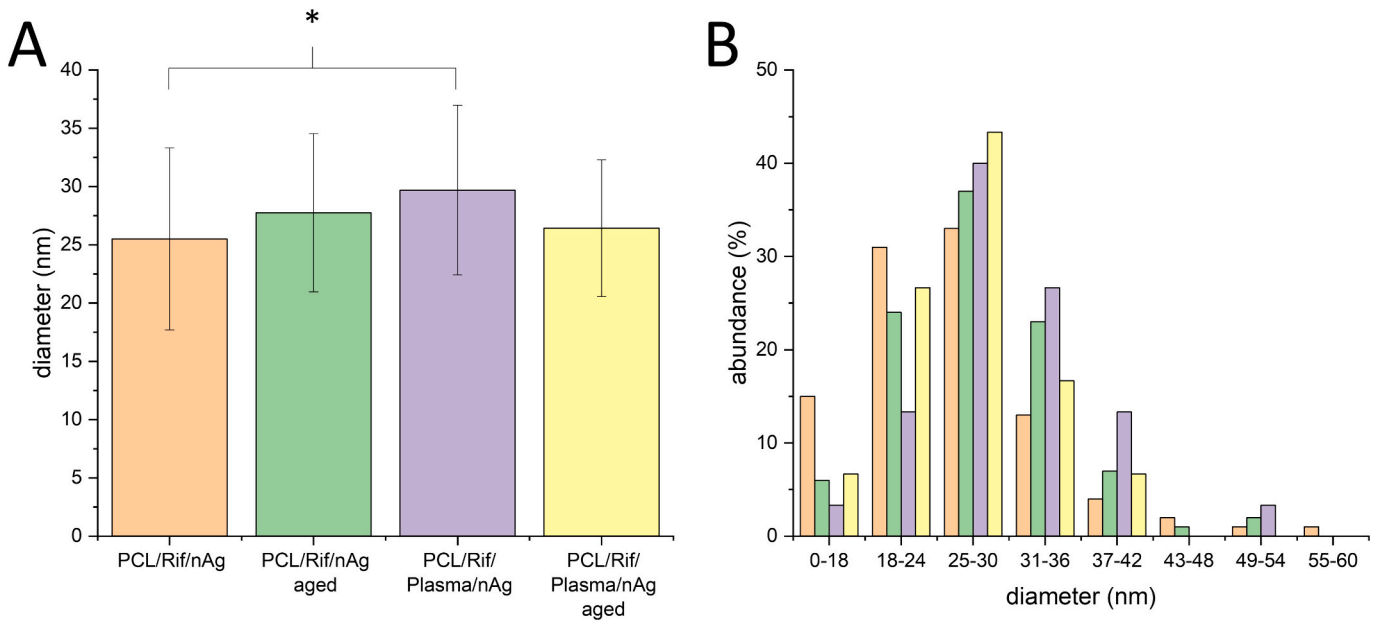

Fig. 8. Dimension analysis of nAg. Average diameter (A) and diameter distribution (B) nAg on PCL/Rif/nAg and PCL/Rif/Plasma/nAg membranes as prepared and after aging in SBF. (*), $p < 0.05$.

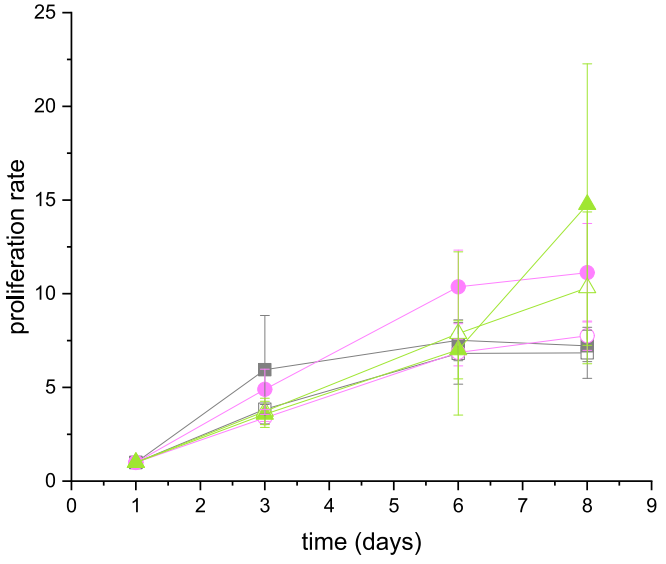

Fig. 9. Proliferation rate of NIH-3 T3 (squares), MG-63 (circles) and UCs (triangles) grown in the absence (empty symbols) or in the presence of PCL/Rif/plasma/nAg (full symbols) membranes.

nanofibrous matrix with homogeneous distribution of diameters, defect-free and with a core-shell morphology. Moreover, the addition of the rifampicin to the process, unlike the rifampicin loaded fibers without a core-shell structure, previously developed [3], did not alter in any way the morphology and the diameter of the nanofibers. It is possible that the addition of the rifampicin to the core solution does not causes a change of the viscosity and conductivity of the polymeric solution allowing the production of core-shell fibers without macroscopic and microscopic defects. The biological application of PCL-based membranes is limited by the intrinsic hydrophobicity of PCL; therefore, PCL and PCL/Rif matrices were subjected to the air-plasma treatment with the purpose to increase their hydrophilicity [70]. This approach had been already successfully applied on PCL and on polylactic acid electrospun membranes and other substrates such as polylactic acid 3D scaffolds and polyetheretherketone surfaces [71–73]. This surface treatment introduces functional chemical groups containing oxygen on the membrane surface, thus increasing its hydrophilicity [9,71,73]. The wettability and surface free energy were examined in the presence of deionized water (DW). Unlike other works where the membranes were subjected to longer treatment [74], a total wettability was observed after only 30 s of air-plasma treatment for both type of membranes. This effect could be due by the strong oxidant activity of the air-plasma cleaning process. Moreover, the increase of the wettability was confirmed by the evaluation of the surface free energy. In detail, thanks to the Owens-Wendt methods, correlating the surface free energy of the polar and dispersive interaction between the surface and the tested fluid [2,61], it was possible to calculate the surface energy and to confirm that the increase of the wettability was due to the introduction of polar groups. With the aim to provide antibacterial properties to the membranes, rifampicin was added to the core solution [75–77]. The rifampicin release from the core of the core-shell fibers was assessed incubating PCL/Rif and PCL/Rif/plasma membranes in PBS. There was a rifampicin burst release from both type of membranes tested in the first 24 h, while at subsequent time points, there was a significant slowdown of the rifampicin released from the membranes, as previously observed [3,13]. This burst release in the surrounding environment may be very helpful in avoiding the bacterial colonization of the membrane surface during its surgical handling and therefore in reducing the risk of the biofilm formation [78,79]. The amount of rifampicin released from both type of the membranes was very similar, proving that the confinement of rifampicin in the fiber core, protected the molecules from the air-plasma treatment, and also that the alteration of the PCL-shell chemistry after the air-plasma treatment did not affect the release of the drug; indeed, the release of rifampicin can be affected by the chemical nature of the molecules that compose the material, as reported by Ashbaugh et al. for rifampicin loaded in PLGA or PCL composites [80]. Moreover, the core-shell morphology could control and slow-down the drug release from nanofibers with respect to rifampicin-loaded nanofibers without a core-shell structure, that on the contrary released relevant amount of the antibiotic in a short time [3]. Beside the factors that affect the release of a drug from nanofibers (concentration, nanofiber composition and dimension, surface area, porosity) [2,81], the release of rifampicin is further affected by the crystallinity of the molecule [82] and by the pH of the medium, displaying a higher release in physiological like

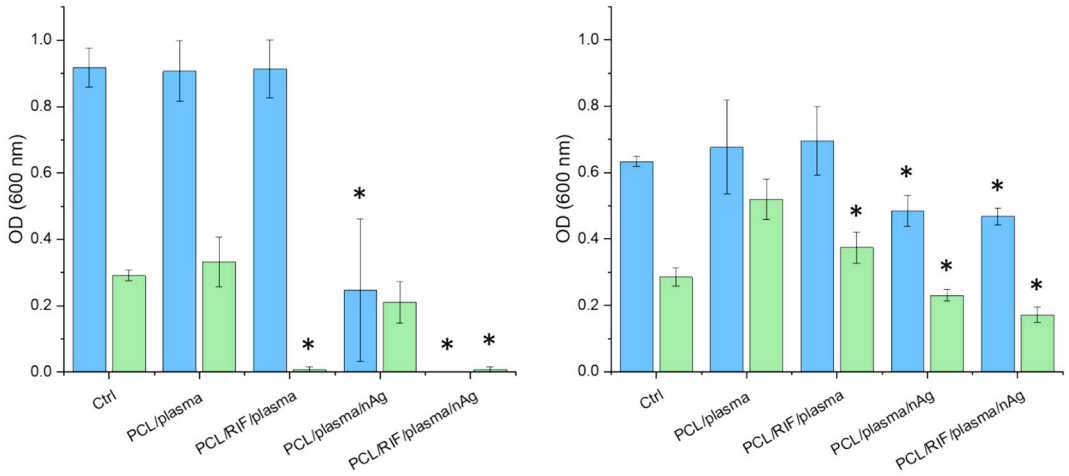

Fig. 10. Inhibition of bacterial growth. Proliferation of *E. coli* ATCC 25922 (blue) and *S. aureus* ATCC 25923-(green) in the presence of freshly prepared membranes (A) and 1-week aged membranes (B). The Ctrl indicates bacterial growth without membranes. Statistically significant differences between the treatments and the Ctrl group for each bacterial strain (Kruskal–Wallis and Mann–Whitney U) are marked with an asterisk (*), $p < 0.05$.

conditions with respect to acidic conditions [83]. We have already reported that the rifampicin loaded in PCL nanofibers is in its amorphous state, thus being more available with respect to the crystal structure [13,82]; moreover, the concentration of the released rifampicin (few μg/mL, data not shown) is lower than the solubility of the rifampicin (few mg/mL in physiological-like conditions [84]), thus indicating that the release is not hampered by the reaching of a saturation condition. Furthermore, comparing the release kinetics of the rifampicin from the PCL nanofibers with the release profiles reported in literature, the same initial burst release followed by a sustained release can be appreciated [77,85,86]. To functionalize the shell of the core-shell fibers, the PCL-based membranes were immersed in a solution of dopamine hydrochloride and silver nitrate to allow the *in-situ* production of silver nanoparticles. This strategy is commonly used thanks to the ability of the dopamine to convert silver ions into silver nanoparticles through the oxidative self-polymerization of the dopamine [87]. SEM images revealed the presence of numerous nano-size silver nanoparticles on the PCL fibers, while the corresponding EDS spectra confirmed the presence of the silver. The SEM analysis did not reveal any differences in the nAg distribution on the surface of the nanofibers depending on the air-plasma treatment, but the dimensional analysis showed that the nanoparticles of PCL/Rif/nAg membranes where slightly bigger than the nAg of PCL/Rif/plasma membranes; this could depend on the different distribution of the polydopamine coating on the membranes, which surface energy is different, and thus on the different synthesis of nAg. The slight increase of nAg diameter observed on aged PCL/Rif/nAg membranes could be due to the early dissolution of smaller nAg; indeed the release of silver from nAg strongly depends on the nAg dimension [88,89]. The release study showed that the membranes are able to release silver ions which are responsible for the antibacterial activity. The release kinetic varies over time and slows down after 24–48 h; this mechanism needs to be better investigated, considering also the high heterogeneity of nAg dimension, but could depend on the passivation of the silver nanoparticles with silver chloride, which hamper the release of silver ions [90]. A comparison of the release kinetics with the literature is not straightforward as several factors vary between the study such as nAg dimension and localization within the nanofibers [88,89]. The electrospun membranes stability after aging in SBF was evaluated up to 8 weeks by SEM investigation revealing that the membranes do not present any morphological defects [68].

In order to assess the antibacterial effectiveness of the developed membranes, in terms of inhibition of the bacterial growth, *E. coli* and *S. aureus* were tested in the presence of the membranes. These bacteria strains represent the main cause of the orthopedic implant-associated infections or infections associated with catheter in the upper urinary tract, and in general of infection affecting soft and hard tissues [91–93]. PCL/plasma/nAg membranes inhibited efficiently the growth of *E. coli*, but not of *S. aureus*. On the opposite, PCL/Rif/plasma strongly inhibited only *S. aureus,* since the rifampicin is particularly effective against this bacterial strain and in general against Gram-positive pathogens [94,95]. However, the rifampicin and the silver ions released by the PCL/Rif/plasma/nAg synergically prevented the growth of both the pathogens with great effectiveness [96]. In the case of *E. coli*, the presence of silver nanoparticles on the shell of the fibers, through a release of silver ions probably acts damages the bacterial envelope and interferes with other essential bacterial processes [97]. Subsequently, the rifampicin released from the core of the fibers could enter the prokaryotic cell.

The aging in SBF decreased the antibacterial activity of membranes due to the reduced amounts of silver nanoparticles and rifampicin. However, compared to the control represented by PCL membranes only, PCL/plasma/nAg and PCL/Rif/plasma/nAg maintained mild inhibitory activity was preserved by the membranes slowing down the growth of *E. coli* and *S. aureus*. Further investigations are needed to optimize the concentration and the release of rifampicin and silver ions in order to reinforce the antibacterial activity overtime, while preserving membranes biocompatibility.

The biocompatibility of all types of matrices was tested in order to exclude the toxicity of rifampicin, silver nanoparticle and of the possible biproducts derived by the air-plasma treatment. Murine fibroblasts (NIH-3 T3), osteosarcoma-derived human osteoblasts (MG-63) and human urothelial bladder carcinoma cells (UC) displayed a good proliferation rate. The lower growth profile displayed by NIH-3 T3 with respect to other cell lines in the presence of all types of membranes between the sixth and the eighth day of culture may not be attributed to membrane toxicity but to reached cell confluency. A similar phenomenon was observed by MG-63 whose proliferation has a constant trend over time until the sixth day, while between the sixth and the eighth day a slowdown of the proliferation was observed. Lastly, unlike of NIH/3 T3 and MG-63, the urotheliocytes showed a constant growth in the presence of all types of matrices until eighth day of culture demonstrating that the solely rifampicin and silver nanoparticles released from the core-shell fibers, as well as their combination, did not causes any cytotoxic effects. Electrospun core-shell membranes with antibacterial activity therefore could represent an emerging and promising approach for tissue engineering applications. In particular, given the versatility of the material, this could be used for the preparation of membranes for guided bone regeneration applications [9] and wound dressings [13], or used as a starting material for the development of electrospun vessel structures

[3]. Further experiments are needed, depending on the final application of the material, to tailor the morphological and mechanical properties of the membranes, to investigate the biological properties in terms of cell differentiation and tissue functionality. Moreover, *in vivo* tests using specific models are needed to investigate the *in vivo* efficacy of the materials, in terms of tissue regeneration and antibacterial efficacy, and the possibility of adverse reactions due to the presence of rifampicin and silver nanoparticles.

5. Conclusions

Double functionalized electrospun core-shell polycaprolactone membranes with antibacterial properties were developed by adding the antibiotic rifampicin in the core region of the nanofibers and by functionalizing with silver nanoparticles the nanofibers surface. The obtained membranes possess a nanofibrous dense matrix without superficial defects; the silver nanoparticle coating is homogeneous over the membrane surface and the release of rifampicin demonstrates that the loading of the rifampicin in the core region protects the molecule from the air-plasma treatment, which increase the membranes hydrophilicity. The membranes are stable over time in physiological-like conditions and are able to release silver ions and rifampicin over time, guaranteeing an antibacterial activity in a synergistic way, while being biocompatible towards different cell lines. The structure of the membranes, the easy functionalization with molecules and compounds of different nature, their antibacterial properties and their biocompatibility, are therefore a starting point for the tuning of the functionality and bioactivity of these membranes, for the development of biomaterials employable in tissue engineering fields where membranes can be useful to isolate an injury or wound site or to build more complex constructs such as vascular structures.

Funding sources

This research did not receive any specific grant from funding agencies in the public, commercial, or not-for-profit sectors.

CRediT authorship contribution statement

Luigi Musciacchio: Writing – original draft, Methodology, Investigation, Conceptualization. **Mario Mardirossian:** Methodology, Investigation. **Giovanna Marussi:** Methodology, Investigation. **Matteo Crosera:** Supervision, Methodology, Investigation. **Gianluca Turco:** Supervision, Project administration. **Davide Porrelli:** Writing – original draft, Supervision, Conceptualization.

Declaration of competing interest

The authors declare that they have no known competing financial interests or personal relationships that could have appeared to influence the work reported in this paper.

Data availability

Data will be made available on request.

Appendix A. Supplementary data

Supplementary data to this article can be found online at https://doi.org/10.1016/j.bioadv.2024.214036.

References

[1] N. Asadi, A.R. Del Bakhshayesh, S. Davaran, A. Akbarzadeh, Common biocompatible polymeric materials for tissue engineering and regenerative medicine, Mater. Chem. Phys. 242 (2020) 122528, https://doi.org/10.1016/j.matchemphys.2019.122528.

[2] M. Gruppuso, B. Guagnini, L. Musciacchio, F. Bellemo, G. Turco, D. Porrelli, Tuning the drug release from antibacterial polycaprolactone/rifampicin-based core–shell electrospun membranes: a proof of concept, ACS Appl. Mater. Interfaces (2022), https://doi.org/10.1021/acsami.2c04849.

[3] L. Musciacchio, M. Mardirossian, B. Guagnini, A. Raffini, M. Rizzo, C. Trombetta, G. Liguori, G. Turco, D. Porrelli, Rifampicin-loaded electrospun polycaprolactone membranes: characterization of stability, antibacterial effects and urotheliocytes proliferation, Mater. Des. 224 (2022) 111286, https://doi.org/10.1016/j.matdes.2022.111286.

[4] T.C. Geremias, M.A. Batistella, R.R.S. Magini, S.M.A. Guelli, U. de Souza, C. V. Franco, L.C.A. Barbosa, U.A. Pereira, J.P. Hinestroza, A.L. Pimenta, A.A. Ulson de Souza, Functionalization of poly(lactic-co-glycolic acid) nanofibrous membranes with antibiofilm compounds, Can. J. Chem. Eng. 100 (2022) S5–S15, https://doi.org/10.1002/cjce.24115.

[5] M. Gruppuso, G. Turco, E. Marsich, D. Porrelli, Polymeric wound dressings, an insight into polysaccharide-based electrospun membranes, Appl. Mater. Today 24 (2021) 101148, https://doi.org/10.1016/j.apmt.2021.101148.

[6] M.E. Talukder, K.M.F. Hasan, J. Wang, J. Yao, C. Li, H. Song, Novel fibrin functionalized multilayered electrospun nanofiber membrane for burn wound treatment, J. Mater. Sci. 56 (2021) 12814–12834, https://doi.org/10.1007/s10853-021-06123-6.

[7] M. Ghazalian, S. Afshar, A. Rostami, S. Rashedi, S.H. Bahrami, Fabrication and characterization of chitosan-polycaprolactone core-shell nanofibers containing tetracycline hydrochloride, Colloids Surf. A Physicochem. Eng. Asp. 636 (2022) 128163, https://doi.org/10.1016/j.colsurfa.2021.128163.

[8] D. Canales, D. Moyano, F. Alvarez, C.D. Grande-Tovar, C.H. Valencia-Llano, L. Peponi, A.R. Boccaccini, P.A. Zapata, Preparation and characterization of novel poly (lactic acid)/calcium oxide nanocomposites by electrospinning as a potential bone tissue scaffold, Biomater. Adv. 153 (2023) 213578, https://doi.org/10.1016/j.bioadv.2023.213578.

[9] D. Porrelli, M. Mardirossian, L. Musciacchio, M. Pacor, F. Berton, M. Crosera, G. Turco, Antibacterial electrospun polycaprolactone membranes coated with polysaccharides and silver nanoparticles for guided bone and tissue regeneration, ACS Appl. Mater. Interfaces 13 (2021) 17255–17267, https://doi.org/10.1021/acsami.1c01016.

[10] J. Jiao, X. Zhao, L. Li, T. Zhu, X. Chen, Q. Ding, Z. Chen, P. Xu, Y. Shi, J. Shao, The promotion of vascular reconstruction by hierarchical structures in biodegradable small-diameter vascular scaffolds, Biomater. Adv. 162 (2024) 213926, https://doi.org/10.1016/j.bioadv.2024.213926.

[11] Z. Zheng, X. Dai, X. Li, C. Du, Functionalization of PCL-based nanofibers loaded with hirudin as blood contact materials, Biomater. Adv. 149 (2023) 213416, https://doi.org/10.1016/j.bioadv.2023.213416.

[12] M.S. Razavi, P. Ebrahimnejad, H.A. Javar, T.A. Weppelmann, J. Akbari, F.A. Amoli, F. Atyabi, R. Dinarvand, Development of dual-functional core-shell electrospun mats with controlled release of anti-inflammatory and anti-bacterial agents for the treatment of corneal alkali burn injuries, Biomater. Adv. 154 (2023) 213648, https://doi.org/10.1016/j.bioadv.2023.213648.

[13] M. Gruppuso, G. Turco, E. Marsich, D. Porrelli, Antibacterial and bioactive multilayer electrospun wound dressings based on hyaluronic acid and lactose-modified chitosan, Biomater. Adv. 154 (2023) 213613, https://doi.org/10.1016/j.bioadv.2023.213613.

[14] M. Wang, R.-L. Ge, F. Zhang, D.-G. Yu, Z.-P. Liu, X. Li, H. Shen, G.R. Williams, Electrospun fibers with blank surface and inner drug gradient for improving sustained release, Biomater. Adv. 150 (2023) 213404, https://doi.org/10.1016/j.bioadv.2023.213404.

[15] A. Gonçalves, B.T. Simões, F.V. Almeida, S.N. Fernandes, M. Valente, T. Vieira, C. Henriques, J.P. Borges, P.I.P. Soares, Engineering dual-stimuli responsive poly (vinyl alcohol) nanofibrous membranes for cancer treatment by magnetic hyperthermia, Biomater. Adv. 145 (2023) 213275, https://doi.org/10.1016/j.bioadv.2022.213275.

[16] L. Sun, J. Zhou, Y. Chen, D.-G. Yu, P. Liu, A combined electrohydrodynamic atomization method for preparing nanofiber/microparticle hybrid medicines, Front. Bioeng. Biotechnol. 11 (2023), https://doi.org/10.3389/fbioe.2023.1308004.

[17] H. Mao, J. Zhou, L. Yan, S. Zhang, D.-G. Yu, Hybrid films loaded with 5-fluorouracil and Reglan for synergistic treatment of colon cancer via asynchronous dual-drug delivery, Front. Bioeng. Biotechnol. 12 (2024), https://doi.org/10.3389/fbioe.2024.1398730.

[18] M. Ruggeri, E. Bianchi, S. Rossi, C. Boselli, A. Icaro Cornaglia, L. Malavasi, R. Carzino, G. Suarato, R. Sánchez-Espejo, A. Athanassiou, C. Viseras, F. Ferrari, G. Sandri, Maltodextrin-amino acids electrospun scaffolds cross-linked with Maillard-type reaction for skin tissue engineering, Biomater. Adv. 133 (2022) 112593, https://doi.org/10.1016/j.msec.2021.112593.

[19] A. Mirek, M. Grzeczkowicz, H. Belaid, A. Bartkowiak, F. Barranger, M. Abid, M. Wasyłeczko, M. Pogorielov, M. Bechelany, D. Lewińska, Electrospun UV-cross-linked polyvinylpyrrolidone fibers modified with polycaprolactone/polyethersulfone microspheres for drug delivery, Biomater. Adv. 147 (2023) 213330, https://doi.org/10.1016/j.bioadv.2023.213330.

[20] D.-G. Yu, W. Gong, J. Zhou, Y. Liu, Y. Zhu, X. Lu, Engineered shapes using electrohydrodynamic atomization for an improved drug delivery, Wiley Interdiscip. Rev. Nanomed. Nanobiotechnol. 16 (2024) e1964, https://doi.org/10.1002/wnan.1964.

[21] Ş.M. Eskitoros-Togay, Y.E. Bulbul, N. Dilsiz, Controlled release of doxycycline within core/shell poly(ε-caprolactone)/poly(ethylene oxide) fibers via coaxial electrospinning, J. Appl. Polym. Sci. 137 (2020) 49273, https://doi.org/10.1002/app.49273.

[22] C. Xu, Y. Cao, C. Lei, Z. Li, T. Kumeria, A.K. Meka, J. Xu, J. Liu, C. Yan, L. Luo, A. Khademhosseini, A. Popat, Y. He, Q. Ye, Polymer–mesoporous silica nanoparticle core–shell nanofibers as a dual-drug-delivery system for guided tissue regeneration, ACS Appl. Nano Mater. 3 (2020) 1457–1467, https://doi.org/10.1021/acsanm.9b02298.
[23] X. Chen, Y. Liu, P. Liu, Electrospun core–sheath nanofibers with a cellulose acetate coating for the synergistic release of zinc ion and drugs, Mol. Pharm. 21 (2024) 173–182, https://doi.org/10.1021/acs.molpharmaceut.3c00703.
[24] C. Qian, Y. Liu, S. Chen, C. Zhang, X. Chen, Y. Liu, P. Liu, Electrospun core–sheath PCL nanofibers loaded with nHA and simvastatin and their potential bone regeneration applications, Front. Bioeng. Biotechnol. 11 (2023), https://doi.org/10.3389/fbioe.2023.1205252.
[25] C. Huang, M. Wang, S. Yu, D.-G. Yu, S.W.A. Bligh, Electrospun fenoprofen/polycaprolactone @ tranexamic acid/hydroxyapatite nanofibers as orthopedic hemostasis dressings, Nanomaterials 14 (2024) 646, https://doi.org/10.3390/nano14070646.
[26] J.G. Edmans, S. Harrison, P.V. Hatton, C. Murdoch, S.G. Spain, H.E. Colley, Electrospinning polymersomes into bead-on-string polyethylene oxide fibres for the delivery of biopharmaceuticals to mucosal epithelia, Biomater. Adv. 157 (2024) 213734, https://doi.org/10.1016/j.bioadv.2023.213734.
[27] S. Chen, J. Zhou, B. Fang, Y. Ying, D.-G. Yu, H. He, Three EHDA processes from a detachable spinneret for fabricating drug fast dissolution composites, Macromol. Mater. Eng. 309 (2024) 2300361, https://doi.org/10.1002/mame.202300361.
[28] J. Zhou, Y. Chen, Y. Liu, T. Huang, J. Xing, R. Ge, D.-G. Yu, Electrospun medicated gelatin/polycaprolactone Janus fibers for photothermal-chem combined therapy of liver cancer, Int. J. Biol. Macromol. 269 (2024) 132113, https://doi.org/10.1016/j.ijbiomac.2024.132113.
[29] P. Zhao, K. Zhou, Y. Xia, C. Qian, D.-G. Yu, Y. Xie, Y. Liao, Electrospun trilayer eccentric Janus nanofibers for a combined treatment of periodontitis, Adv. Fiber Mater. (2024), https://doi.org/10.1007/s42765-024-00397-6.
[30] Y. Shi, Y. Zhang, L. Zhu, Y. Miao, Y. Zhu, B. Yue, Tailored drug delivery platforms: stimulus-responsive core–shell structured nanocarriers, Adv. Healthc. Mater. 13 (2024) 2301726, https://doi.org/10.1002/adhm.202301726.
[31] S. Yan, Y. Qian, M. Haghayegh, Y. Xia, S. Yang, R. Cao, M. Zhu, Electrospun organic/inorganic hybrid nanofibers for accelerating wound healing: a review, J. Mater. Chem. B 12 (2024) 3171–3190, https://doi.org/10.1039/D4TB00149D.
[32] X. Zhang, N. Yu, Q. Ren, S. Niu, L. Zhu, L. Hong, K. Cui, X. Wang, W. Jiang, M. Wen, Z. Chen, Janus nanofiber membranes with photothermal-enhanced biofluid drainage and sterilization for diabetic wounds, Adv. Funct. Mater. 34 (2024) 2315020, https://doi.org/10.1002/adfm.202315020.
[33] Y. Sun, J. Zhou, Z. Zhang, D.-G. Yu, S.W.A. Bligh, Integrated Janus nanofibers enabled by a co-shell solvent for enhancing icariin delivery efficiency, Int. J. Pharm. 658 (2024) 124180, https://doi.org/10.1016/j.ijpharm.2024.124180.
[34] J. Zhou, T. Yi, Z. Zhang, D.-G. Yu, P. Liu, L. Wang, Y. Zhu, Electrospun Janus core (ethyl cellulose//polyethylene oxide) @ shell (hydroxypropyl methyl cellulose acetate succinate) hybrids for an enhanced colon-targeted prolonged drug absorbance, Adv. Compos. Hybrid Mater. 6 (2023) 189, https://doi.org/10.1007/s42114-023-00766-6.
[35] L. Xu, Q. Li, H. Wang, H. Liu, D.-G. Yu, S.-W.A. Bligh, X. Lu, Electrospun multifunctional medicated tri-section Janus nanofibers for an improved anti-adhesion tendon repair, Chem. Eng. J. 492 (2024) 152359, https://doi.org/10.1016/j.cej.2024.152359.
[36] S.N. Kalva, R. Augustine, A. Al Mamun, Y.B. Dalvi, N. Vijay, A. Hasan, Active agents loaded extracellular matrix mimetic electrospun membranes for wound healing applications, J. Drug Deliv. Sci. Technol. 63 (2021) 102500, https://doi.org/10.1016/j.jddst.2021.102500.
[37] G. Amokrane, V. Humblot, E. Jubeli, N. Yagoubi, S. Ramtani, V. Migonney, C. Falentin-Daudré, Electrospun poly(ε-caprolactone) fiber scaffolds functionalized by the covalent grafting of a bioactive polymer: surface characterization and influence on in vitro biological response, ACS Omega 4 (2019) 17194–17208, https://doi.org/10.1021/acsomega.9b01647.
[38] B. Liu, T. Yao, L. Ren, Y. Zhao, X. Yuan, Antibacterial PCL electrospun membranes containing synthetic polypeptides for biomedical purposes, Colloids Surf. B. Biointerfaces 172 (2018) 330–337, https://doi.org/10.1016/j.colsurfb.2018.08.055.
[39] M. Liu, R. Wang, J. Liu, W. Zhang, Z. Liu, X. Lou, H. Nie, H. Wang, X. Mo, A.I. Abd-Elhamid, R. Zheng, J. Wu, Incorporation of magnesium oxide nanoparticles into electrospun membranes improves pro-angiogenic activity and promotes diabetic wound healing, Biomater. Adv. 133 (2022) 112609, https://doi.org/10.1016/j.msec.2021.112609.
[40] T.G. Darshan, C.-H. Chen, C.-Y. Kuo, K.T. Shalumon, Y.-M. Chien, H.-H. Kao, J.-P. Chen, Development of high resilience spiral wound suture-embedded gelatin/PCL/heparin nanofiber membrane scaffolds for tendon tissue engineering, Int. J. Biol. Macromol. 221 (2022) 314–333, https://doi.org/10.1016/j.ijbiomac.2022.09.001.
[41] Z. Wang, X. Song, Y. Cui, K. Cheng, X. Tian, M. Dong, L. Liu, Silk fibroin H-fibroin/poly(ε-caprolactone) core-shell nanofibers with enhanced mechanical property and long-term drug release, J. Colloid Interface Sci. 593 (2021) 142–151, https://doi.org/10.1016/j.jcis.2021.02.099.
[42] M. Abasalta, A. Asefnejad, M.T. Khorasani, A.R. Saadatabadi, M. Irani, Adsorption and sustained release of doxorubicin from N-carboxymethyl chitosan/polyvinyl alcohol/poly(ε-caprolactone) composite and core-shell nanofibers, J. Drug Deliv. Sci. Technol. 67 (2022) 102937, https://doi.org/10.1016/j.jddst.2021.102937.
[43] M.A. Mohamady Hussein, E. Guler, E. Rayaman, M.E. Cam, A. Sahin, M. Grinholc, D. Sezgin Mansuroglu, Y.M. Sahin, O. Gunduz, M. Muhammed, I.M. El-Sherbiny, M. Megahed, Dual-drug delivery of ag-chitosan nanoparticles and phenytoin via core-shell PVA/PCL electrospun nanofibers, Carbohydr. Polym. 270 (2021) 118373, https://doi.org/10.1016/j.carbpol.2021.118373.
[44] A.F. Martins, S.P. Facchi, P.C.F. da Câmara, S.E.A. Camargo, C.H.R. Camargo, K. C. Popat, M.J. Kipper, Novel poly(ε-caprolactone)/amino-functionalized tannin electrospun membranes as scaffolds for tissue engineering, J. Colloid Interface Sci. 525 (2018) 21–30, https://doi.org/10.1016/j.jcis.2018.04.060.
[45] F. Ahmad, N. Ashraf, M.I. Elahi, Y. Zhou, Y. Lu, D.-C. Yin, Fabrication of biogenic-silver nanoparticles functionalized electrospun membranes counteracting bacteria and enhance wound healing, Mater. Today Commun. 31 (2022) 103493, https://doi.org/10.1016/j.mtcomm.2022.103493.
[46] G. Lopes Gama E. Silva, M. Sato de Souza de Bustamante Monteiro, M. Lopes Dias, A. Machado Costa, A. Malta Rossi, A. Paula dos Santos Matos, R. Santos-Oliveira, E. Ricci-Junior, Antibiotics-loaded nanofibers fabricated by electrospinning for the treatment of bone infections, Arab. J. Chem. 16 (2023) 104392, https://doi.org/10.1016/j.arabjc.2022.104392.
[47] S. Wu, Y. Huang, J. Yan, Y. Li, J. Wang, Y.Y. Yang, P. Yuan, X. Ding, Bacterial outer membrane-coated mesoporous silica nanoparticles for targeted delivery of antibiotic rifampicin against gram-negative bacterial infection in vivo, Adv. Funct. Mater. 31 (2021) 2103442, https://doi.org/10.1002/adfm.202103442.
[48] S. Maghrebi, P. Joyce, M. Jambhrunkar, N. Thomas, C.A. Prestidge, Poly(lactic-co-glycolic) acid–lipid hybrid microparticles enhance the intracellular uptake and antibacterial activity of rifampicin, ACS Appl. Mater. Interfaces 12 (2020) 8030–8039, https://doi.org/10.1021/acsami.9b22991.
[49] P. Joyce, H. Ulmefors, S. Maghrebi, S. Subramaniam, A. Wignall, S. Jõemetsa, F. Höök, C.A. Prestidge, Enhancing the cellular uptake and antibacterial activity of rifampicin through encapsulation in mesoporous silica nanoparticles, Nanomaterials 10 (2020) 815, https://doi.org/10.3390/nano10040815.
[50] D. Abdelmoneim, D. Coates, G. Porter, P. Schmidlin, K.C. Li, S. Botter, K. Lim, W. Duncan, In vitro and in vivo investigation of antibacterial silver nanoparticles functionalized bone grafting substitutes, J. Biomed. Mater. Res. A n/a (2024), https://doi.org/10.1002/jbm.a.37757.
[51] Z. Vilamová, Z. Šimonová, J. Bednář, P. Mikeš, M. Cieslar, L. Svoboda, R. Dvorský, K. Rosenbergová, G. Kratošová, Silver-loaded poly(vinyl alcohol)/polycaprolactone polymer scaffold as a biocompatible antibacterial system, Sci. Rep. 14 (2024) 11093, https://doi.org/10.1038/s41598-024-61567-5.
[52] S. Dugam, R. Jain, P. Dandekar, Silver nanoparticles loaded triple-layered cellulose-acetate based multifunctional dressing for wound healing, Int. J. Biol. Macromol. 276 (2024) 133837, https://doi.org/10.1016/j.ijbiomac.2024.133837.
[53] A. Wali, M. Gorain, G. Kundu, M. Badiger, Silver nanoparticles in electrospun ethyl hydroxy ethyl cellulose-PVA nanofiber: synthesis, characterization and wound dressing applications, Carbohydr. Polym. Technol. Appl. 7 (2024) 100477, https://doi.org/10.1016/j.carpta.2024.100477.
[54] H. Mufty, J. Van Den Eynde, B. Meuris, W.-J. Metsemakers, E. Van Wijngaerden, T. Vandendriessche, H.P. Steenackers, I. Fourneau, Pre-clinical *in vitro* models of vascular graft coating in the prevention of vascular graft infection: a systematic review, Eur. J. Vasc. Endovasc. Surg. 63 (2022) 119–137, https://doi.org/10.1016/j.ejvs.2021.07.015.
[55] S. Patil, N. Singh, Antibacterial silk fibroin scaffolds with green synthesized silver nanoparticles for osteoblast proliferation and human mesenchymal stem cell differentiation, Colloids Surf. B. Biointerfaces 176 (2019) 150–155, https://doi.org/10.1016/j.colsurfb.2018.12.067.
[56] M. Godoy-Gallardo, U. Eckhard, L.M. Delgado, Y.J.D. de Roo Puente, M. Hoyos-Nogués, F.J. Gil, R.A. Perez, Antibacterial approaches in tissue engineering using metal ions and nanoparticles: from mechanisms to applications, Bioact. Mater. 6 (2021) 4470–4490, https://doi.org/10.1016/j.bioactmat.2021.04.033.
[57] H. Deng, D. McShan, Y. Zhang, S.S. Sinha, Z. Arslan, P.C. Ray, H. Yu, Mechanistic study of the synergistic antibacterial activity of combined silver nanoparticles and common antibiotics, Environ. Sci. Technol. 50 (2016) 8840–8848, https://doi.org/10.1021/acs.est.6b00998.
[58] R. Vazquez-Muñoz, A. Meza-Villezcas, P.G.J. Fournier, E. Soria-Castro, K. Juarez-Moreno, A.L. Gallego-Hernández, N. Bogdanchikova, R. Vazquez-Duhalt, A. Huerta-Saquero, Enhancement of antibiotics antimicrobial activity due to the silver nanoparticles impact on the cell membrane, PloS One 14 (2019) e0224904, https://doi.org/10.1371/journal.pone.0224904.
[59] H.Y. Son, J.H. Ryu, H. Lee, Y.S. Nam, Silver-polydopamine hybrid coatings of electrospun poly(vinyl alcohol) nanofibers, Macromol. Mater. Eng. 298 (2013) 547–554, https://doi.org/10.1002/mame.201200231.
[60] Z. Yang, Y. Wu, J. Wang, B. Cao, C.Y. Tang, In situ reduction of silver by polydopamine: a novel antimicrobial modification of a thin-film composite polyamide membrane, Environ. Sci. Technol. 50 (2016) 9543–9550, https://doi.org/10.1021/acs.est.6b01867.
[61] D.K. Owens, Estimation of the surface free energy of polymers, J. Appl. Polym. Sci. 13 (1969) 1741–1747, https://doi.org/10.1002/app.1969.070130815.
[62] Z. Ren, G. Chen, Z. Wei, L. Sang, M. Qi, Hemocompatibility evaluation of polyurethane film with surface-grafted poly(ethylene glycol) and carboxymethyl-chitosan, J. Appl. Polym. Sci. 127 (2013) 308–315, https://doi.org/10.1002/app.37885.
[63] L.A. Can-Herrera, A. Ávila-Ortega, S. de la Rosa-García, A.I. Oliva, J.V. Cauich-Rodríguez, J.M. Cervantes-Uc, Surface modification of electrospun polycaprolactone microfibers by air plasma treatment: effect of plasma power and treatment time, Eur. Polym. J. 84 (2016) 502–513, https://doi.org/10.1016/j.eurpolymj.2016.09.060.
[64] T. Kokubo, H. Kushitani, S. Sakka, T. Kitsugi, T. Yamamuro, Solutions able to reproduce in vivo surface-structure changes in bioactive glass-ceramic A-W3, J. Biomed. Mater. Res. 24 (1990) 721–734, https://doi.org/10.1002/jbm.820240607.

[65] B. Guagnini, B. Medagli, B. Zumbo, V. Cannillo, G. Turco, D. Porrelli, D. Bellucci, Alginate-Sr/mg containing bioactive glass scaffolds: the characterization of a new 3D composite for bone tissue engineering, J. Funct. Biomater. 15 (2024) 183, https://doi.org/10.3390/jfb15070183.
[66] W. Guo, M. Chen, Z. Wang, Y. Tian, J. Zheng, S. Gao, Y. Li, Y. Zheng, X. Li, J. Huang, W. Niu, S. Jiang, C. Hao, Z. Yuan, Y. Zhang, M. Wang, Z. Wang, J. Peng, A. Wang, Y. Wang, X. Sui, W. Xu, L. Hao, X. Zheng, S. Liu, Q. Guo, 3D-printed cell-free PCL–MECM scaffold with biomimetic micro-structure and micro-environment to enhance in situ meniscus regeneration, Bioact. Mater. 6 (2021) 3620–3633, https://doi.org/10.1016/j.bioactmat.2021.02.019.
[67] S. Behtaj, F. Karamali, E. Masaeli, Y.G. Anissimov, M. Rybachuk, Electrospun PGS/PCL, PLLA/PCL, PLGA/PCL and pure PCL scaffolds for retinal progenitor cell cultivation, Biochem. Eng. J. 166 (2021) 107846, https://doi.org/10.1016/j.bej.2020.107846.
[68] J.R. Dias, A. Sousa, A. Augusto, P.J. Bártolo, P.L. Granja, Electrospun polycaprolactone (PCL) degradation: an in vitro and in vivo study, Polymers 14 (2022) 3397, https://doi.org/10.3390/polym14163397.
[69] H. Nazari, A. Heirani-Tabasi, E. Esmaeili, A.-M. Kajbafzadeh, Z. Hassannejad, S. Boroomand, M.H. Shahsavari Alavijeh, M.A. Mishan, S.H. Ahmadi Tafti, M. E. Warkiani, N. Dadgar, Decellularized human amniotic membrane reinforced by MoS2-polycaprolactone nanofibers, a novel conductive scaffold for cardiac tissue engineering, J. Biomater. Appl. 36 (2022) 1527–1539, https://doi.org/10.1177/08853282211063289.
[70] N. Recek, M. Resnik, H. Motaln, T. Lah-Turnšek, R. Augustine, N. Kalarikkal, S. Thomas, M. Mozetič, Cell adhesion on polycaprolactone modified by plasma treatment, Int. J. Polym. Sci. 2016 (2016) e7354396, https://doi.org/10.1155/2016/7354396.
[71] F. Lopresti, S. Campora, G. Tirri, E. Capuana, F. Carfì Pavia, V. Brucato, G. Ghersi, V. La Carrubba, Core-shell PLA/Kef hybrid scaffolds for skin tissue engineering applications prepared by direct kefiran coating on PLA electrospun fibers optimized via air-plasma treatment, Mater. Sci. Eng. C 127 (2021) 112248, https://doi.org/10.1016/j.msec.2021.112248.
[72] V.M. Vijayan, M. Walker, R.R. Pillai, G.H. Moreno, Y.K. Vohra, J.J. Morris, V. Thomas, Plasma electroless reduction: a green process for designing metallic nanostructure interfaces onto polymeric surfaces and 3D scaffolds, ACS Appl. Mater. Interfaces 14 (2022) 25065–25079, https://doi.org/10.1021/acsami.2c01195.
[73] D. Porrelli, M. Mardirossian, N. Crapisi, M. Urban, N.A. Ulian, L. Bevilacqua, G. Turco, M. Maglione, Polyetheretherketone and titanium surface treatments to modify roughness and wettability – improvement of bioactivity and antibacterial properties, J. Mater. Sci. Technol. 95 (2021) 213–224, https://doi.org/10.1016/j.jmst.2021.04.023.
[74] L.A. Can-Herrera, A.I. Oliva, J.M. Cervantes-Uc, Enhancement of chemical, physical, and surface properties of electrospun PCL/PLA blends by means of air plasma treatment, Polym. Eng. Sci. 62 (2022) 1608–1618, https://doi.org/10.1002/pen.25949.
[75] S.P. Carneiro, K.V. Carvalho, R.D. de Oliveira Aguiar Soares, C.M. Carneiro, M.H.G. de Andrade, R.S. Duarte, O.D.H. dos Santos, Functionalized rifampicin-loaded nanostructured lipid carriers enhance macrophages uptake and antimycobacterial activity, Colloids Surf. B 175 (2019) 306–313. doi:https://doi.org/10.1016/j.colsurfb.2018.12.003.
[76] E. Snejdrova, J. Loskot, J. Martiska, T. Soukup, L. Prokes, V. Frolov, T. Kucera, Rifampicin-loaded PLGA nanoparticles for local treatment of musculoskeletal infections: formulation and characterization, J. Drug Deliv. Sci. Technol. 73 (2022) 103435, https://doi.org/10.1016/j.jddst.2022.103435.
[77] T.T. Ruckh, R.A. Oldinski, D.A. Carroll, K. Mikhova, J.D. Bryers, K.C. Popat, Antimicrobial effects of nanofiber poly(caprolactone) tissue scaffolds releasing rifampicin, J. Mater. Sci. Mater. Med. 23 (2012) 1411–1420, https://doi.org/10.1007/s10856-012-4609-3.
[78] K. Horprasertkij, A. Dwivedi, K. Riansuwan, P. Kiratisin, N. Nasongkla, Spray coating of dual antibiotic-loaded nanospheres on orthopedic implant for prolonged release and enhanced antibacterial activity, J. Drug Deliv. Sci. Technol. 53 (2019) 101102, https://doi.org/10.1016/j.jddst.2019.05.051.
[79] V. Ständert, K. Borcherding, N. Bormann, G. Schmidmaier, I. Grunwald, B. Wildemann, Antibiotic-loaded amphora-shaped pores on a titanium implant surface enhance osteointegration and prevent infections, Bioact. Mater. 6 (2021) 2331–2345, https://doi.org/10.1016/j.bioactmat.2021.01.012.
[80] A.G. Ashbaugh, X. Jiang, J. Zheng, A.S. Tsai, W.-S. Kim, J.M. Thompson, R. J. Miller, J.H. Shahbazian, Y. Wang, C.A. Dillen, A.A. Ordonez, Y.S. Chang, S. K. Jain, L.C. Jones, R.S. Sterling, H.-Q. Mao, L.S. Miller, Polymeric nanofiber coating with tunable combinatorial antibiotic delivery prevents biofilm-associated infection in vivo, Proc. Natl. Acad. Sci. 113 (2016) E6919–E6928, https://doi.org/10.1073/pnas.1613722113.
[81] R. Jiffrin, S.I.A. Razak, M.I. Jamaludin, A.S.A. Hamzah, M.A. Mazian, M.A.T. Jaya, M.Z. Nasrullah, M. Majrashi, A. Theyab, A.A. Aldarmahi, Z. Awan, M.M. Abdel-Daim, A.K. Azad, Electrospun nanofiber composites for drug delivery: a review on current progresses, Polymers 14 (2022) 3725, https://doi.org/10.3390/polym14183725.
[82] P. Khadka, S. Sinha, I.G. Tucker, J. Dummer, P.C. Hill, R. Katare, S.C. Das, Pharmacokinetics of rifampicin after repeated intra-tracheal administration of amorphous and crystalline powder formulations to Sprague Dawley rats, Eur. J. Pharm. Biopharm. 162 (2021) 1–11, https://doi.org/10.1016/j.ejpb.2021.02.011.
[83] L. Miranda-Calderon, C. Yus, C. Remirez de Ganuza, M. Paesa, G. Landa, E. Tapia, E. Pérez, M. Perez, V. Sebastian, S. Irusta, G. Mendoza, M. Arruebo, Combinatorial wound dressings loaded with synergistic antibiotics in the treatment of chronic infected wounds, Chem. Eng. J. 476 (2023) 146679, https://doi.org/10.1016/j.cej.2023.146679.
[84] S. Agrawal, R. Panchagnula, Implication of biopharmaceutics and pharmacokinetics of rifampicin in variable bioavailability from solid oral dosage forms, Biopharm. Drug Dispos. 26 (2005) 321–334, https://doi.org/10.1002/bdd.464.
[85] C. Li, Y. Liu, M. Wei, J. Liu, X. Yu, P. Hu, Y. Liu, A novel core-shell rifampicin/isoniazid electrospun nanofiber membrane for long time drug dissolution, Eng. Regen. 3 (2022) 73–79, https://doi.org/10.1016/j.engreg.2022.02.002.
[86] S.E. Gilchrist, D. Lange, K. Letchford, H. Bach, L. Fazli, H.M. Burt, Fusidic acid and rifampicin co-loaded PLGA nanofibers for the prevention of orthopedic implant associated infections, J. Control. Release 170 (2013) 64–73, https://doi.org/10.1016/j.jconrel.2013.04.012.
[87] H.A. Tran, P.A. Tran, In situ coatings of silver nanoparticles for biofilm treatment in implant-retention surgeries: antimicrobial activities in monoculture and coculture, ACS Appl. Mater. Interfaces 13 (2021) 41435–41444, https://doi.org/10.1021/acsami.1c08239.
[88] C. Zhang, X. Yang, L. Yu, X. Chen, J. Zhang, S. Zhang, S. Wu, Electrospun polyasparthydrazide nanofibrous hydrogel loading with in-situ synthesized silver nanoparticles for full-thickness skin wound healing application, Mater. Des. 239 (2024) 112818, https://doi.org/10.1016/j.matdes.2024.112818.
[89] Z. Mahdieh, S. Mitra, A. Holian, Core–shell electrospun fibers with an improved open pore structure for size-controlled delivery of nanoparticles, ACS Appl. Polym. Mater. 2 (2020) 4004–4015, https://doi.org/10.1021/acsapm.0c00643.
[90] K. Loza, J. Diendorf, C. Sengstock, L. Ruiz-Gonzalez, J.M. Gonzalez-Calbet, M. Vallet-Regi, M. Köller, M. Epple, The dissolution and biological effects of silver nanoparticles in biological media, J. Mater. Chem. B 2 (2014) 1634–1643, https://doi.org/10.1039/C3TB21569E.
[91] J.L.P. Gemeinder, N.R. de Barros, G.S. Pegorin, J.L. de Singulani, F.A. Borges, M.C. G.D. Arco, M.J.S.M. Giannini, A.M.F. Almeida, S.L.S. de Salvador, R.D. Herculano, Gentamicin encapsulated within a biopolymer for the treatment of Staphylococcus aureus and Escherichia coli infected skin ulcers, J. Biomater. Sci. Polym. Ed. 32 (2021) 93–111, https://doi.org/10.1080/09205063.2020.1817667.
[92] J. Barros, L.D.R. Melo, P. Poeta, G. Igrejas, M.P. Ferraz, J. Azeredo, F.J. Monteiro, Lytic bacteriophages against multidrug-resistant Staphylococcus aureus, enterococcus faecalis and Escherichia coli isolates from orthopaedic implant-associated infections, Int. J. Antimicrob. Agents 54 (2019) 329–337, https://doi.org/10.1016/j.ijantimicag.2019.06.007.
[93] M. Kar, A. Dubey, S.S. Patel, T. Siddiqui, U. Ghoshal, C. Sahu, Characteristics of bacterial colonization and urinary tract infection after indwelling of double-J ureteral stent and percutaneous nephrostomy tube, J. Glob. Infect. Dis. 14 (2022) 75, https://doi.org/10.4103/jgid.jgid_276_21.
[94] A. Valliammai, A. Selvaraj, U. Yuvashree, C. Aravindraja, S., Karutha Pandian, sarA-dependent antibiofilm activity of thymol enhances the antibacterial efficacy of rifampicin against Staphylococcus aureus, Front. Microbiol. 11 (2020) 1744, https://doi.org/10.3389/fmicb.2020.01744.
[95] H. Suzuki, M. Goto, R. Nair, D.J. Livorsi, P. Sekar, M.E. Ohl, D.J. Diekema, E. N. Perencevich, B. Alexander, M.P. Jones, J.S. McDaniel, M.L. Schweizer, Effectiveness and optimal duration of adjunctive rifampin treatment in the management of Staphylococcus aureus prosthetic joint infections after debridement, antibiotics, and implant retention, Open Forum Infect. Dis. 9 (2022) ofac473, https://doi.org/10.1093/ofid/ofac473.
[96] D. Yu, J. Xu, R. Li, J. Zhao, F. Li, Y. Zhai, J. Xue, H. Song, F. Yang, P. Xu, Y. Song, Synergetic effect of rifampin loaded mussel-inspired silver nanoparticles for enhanced antibacterial activity against multidrug-resistant strain of mycobacterium tuberculosis, ChemistrySelect 6 (2021) 10682–10687, https://doi.org/10.1002/slct.202101973.
[97] B. Hosnedlova, D. Kabanov, M. Kepinska, V.H.B. Narayanan, A.A. Parikesit, C. Fernandez, G. Bjørklund, H.V. Nguyen, A. Farid, J. Sochor, A. Pholosi, M. Baron, M. Jakubek, R. Kizek, Effect of biosynthesized silver nanoparticles on bacterial biofilm changes in *S. aureus* and *E. coli*, Nanomaterials 12 (2022) 2183, https://doi.org/10.3390/nano12132183.